HHS Public Access

Author manuscript

Sci Signal. Author manuscript; available in PMC 2021 December 22.

Published in final edited form as:

Sci Signal. ; 14(688): . doi:10.1126/scisignal.abd2464.

Combinatorial phosphorylation modulates the structure and function of the G protein γ subunit in yeast

Zahra Nassiri Toosi[1], **Xinya Su**[1], **Ruth Austin**[1], **Shilpa Choudhury**[1], **Wei Li**[1,2], **Yui Tik Pang**[3], **James C. Gumbart**[3], **Matthew P. Torres**[1,2,*]

[1]School of Biological Sciences; Georgia Institute of Technology; Atlanta, GA 30332, USA.

[2]Southeast Center for Mathematics and Biology, Georgia Institute of Technology; Atlanta, GA 30332, USA.

[3]School of Physics; Georgia Institute of Technology; Atlanta, GA 30332, USA.

Abstract

Intrinsically disordered regions (IDRs) in proteins are often targets of combinatorial posttranslational modifications, which serve to regulate protein structure and function. Emerging evidence suggests that the N-terminal tails of G protein γ subunits, which are essential components of heterotrimeric G proteins, are intrinsically disordered, phosphorylation-dependent determinants of G protein signaling. Here, we found that the yeast Gγ subunit Ste18 underwent combinatorial, multisite phosphorylation events within its N-terminal IDR. G protein–coupled receptor (GPCR) activation and osmotic stress induced phosphorylation at Ser^7, whereas glucose and acid stress induced phosphorylation at Ser^3, which was a quantitative indicator of intracellular pH. Each site was phosphorylated by a distinct set of kinases, and phosphorylation of one site affected phosphorylation of the other, as determined through exposure to serial stimuli and through phosphosite mutagenesis. Lastly, we showed that phosphorylation resulted in changes in IDR structure and that different combinations of phosphorylation events modulated the activation rate and amplitude of the downstream mitogen-activated protein kinase Fus3. These data place Gγ subunits among intrinsically disordered proteins that undergo combinatorial posttranslational modifications that govern signaling pathway output.

Introduction

Combinatorial posttranslational modification (PTM) of intrinsically disordered protein termini has emerged as a prominent regulatory feature in protein biology. Indeed, there are several well-characterized examples in which the core regulatory element is defined by three criteria: the N- or C-terminal location of an intrinsically disordered region (IDR); the dynamic and combinatorial modification of amino acid sidechains within the IDR;

*Corresponding author. mtorres35@gatech.edu.

Author contributions: Z.N.T., X.S., R.A., S.C., and W.L. performed experiments. Y.T.P. and J.G. performed MD simulations. Z.N.T. and M.T. wrote the manuscript.

Competing interests: The authors declare that they have no competing interests.

Data and materials availability: All data needed to evaluate the conclusions in the paper are present in the paper or the Supplementary Materials.

and the propensity for such changes to alter protein-protein interactions and functional output. Prominent examples include the N-terminal tails of histone proteins, which undergo complex combinatorial PTMs that affect eukaryotic gene transcription (1); the C-terminal domain of RNA polymerase II, which undergoes dynamic, site-specific phosphorylation that modulates transcription initiation and elongation (2); the C-terminal tails of tubulin, which undergo combinatorial modifications that coordinate microtubule–end protein interactions (3); the C-terminal tails of G protein–coupled receptors (GPCRs), which undergo barcode-like phosphorylation that coordinates protein-protein interactions that determine pathway selectivity in G protein signaling (4–6); and other well-known examples that are also conserved across eukaryotes from yeast to humans (7, 8). In this work, we tested the hypothesis that heterotrimeric G protein γ subunits (Gγ), small, yet essential, GPCR signal–transducing proteins with N-terminal IDR phosphorylation hotspots, undergo regulatory combinatorial phosphorylation similar to that of classically defined PTM-regulated terminal IDRs.

Heterotrimeric guanine nucleotide–binding proteins (G proteins), an evolutionarily conserved group of protein families consisting of Gα, Gβ, and Gγ subunits, function as transducers of extracellular signals, such as light, hormones, and neurotransmitters, which activate seven-transmembrane domain GPCRs embedded within the plasma membrane of eukaryotic cells (9). Activation of the GPCR on its extracellular surface stimulates a conformational change in the Gα subunit that promotes guanine nucleotide exchange and facilitates its dissociation from Gβγ, an obligate heterodimer of Gβ and Gγ subunits. Once dissociated, both Gα and Gβγ are free to interact with and modulate the activities of downstream protein effectors that control the production of second messenger signals, the activation of kinases, and the coordination of macromolecular events that constitute the cellular response to the stimulus. Signaling continues until Gα hydrolyzes GTP to generate GDP and re-enters a conformation that sequesters Gβγ, a process that is accelerated by the interaction of Gα subunits with regulators of G protein (RGS) proteins (10).

As the smaller members of the obligate Gβγ heterodimer, Gγ subunits are often thought to have limited functionality as membrane anchors for Gβ subunits, a function mediated through lipidation of C-terminal cysteine residues and through coiled-coil interactions with the N-terminal residues of Gβ subunits (11–13). However, evidence suggests that the N-terminal regions of Gβ and Gγ, which are proximal to each other in the Gβγ dimer, play an important role in Gβγ-dependent effector signaling. In the budding yeast *Saccharomyces cerevisiae* (yeast), the effector-binding sites on Gβγ are located in N-terminal residues in $G\beta_{Ste4}$ (14, 15), which overlap with the same region in human $G\beta_1\gamma_2$ that inhibits phospholipase C β2 activity in mammals (16). Mutation near this region modulates mammalian Gβγ-dependent activity of adenylyl cyclase 5 (AC5) and AC6 in vitro (17).

The extreme N-termini of Gγ subunits are intrinsically disordered phosphorylation hotspots that govern Gβγ-effector interactions and activity (18, 19). Meta-proteomic informatics analysis showed that Gγ subunits harbor two-fold greater modification density (average number of PTMs per total protein length in residue number) than Gα or Gβ subunits, RGS proteins, or GPCRs (19, 20). Moreover, all Gγ subunits throughout Eukarya harbor an N-terminal IDR. Within this IDR, which averages between 7 and 13 residues in length,

most Gγ proteins harbor at least two phospho-acceptor residues and approximately 60% of all experimentally observed Gγ phosphorylation events; 12 times more than what is observed outside the N-terminal IDR (19). Previous work in mammals first demonstrated that protein kinase C (PKC)–dependent phosphorylation within this hotspot in $G\gamma_{12}$ inhibits AC2 stimulation by $G\beta_1\gamma_{12}$ in vitro (21) and is required for normal fibroblast motility in vivo (22).

N-terminal Gγ phosphorylation is also required for G protein signaling in yeast. The budding yeast Gγ subunit Ste18 undergoes mitogen-activated protein kinase (MAPK)-dependent feedback phosphorylation within its N-terminal IDR in response to pheromone-dependent activation of the pheromone GPCR, Ste2 (18). The Ste18 N-terminal IDR harbors three phospho-acceptor residues (Thr^2, Ser^3, and Ser^7), and nullification of all three sites by mutation to alanine (S/T-A), in combination with hyperactivating mutations in the Gβγ effector and MAPK scaffold, Ste5, results in rapid and prolonged bulk-accumulation of the scaffold at the plasma membrane and subsequent ultra-fast and enhanced activation of the terminal MAPK, Fus3. In contrast, phosphomimic mutation of the same residues to glutamate (S/T-E) results in normal plasma membrane recruitment of Ste5 and subsequent MAPK activation. These data suggested to us that, like other PTM-regulatory terminal IDRs, phosphorylation within the N-termini of Gγ subunits might serve to govern their protein interactions and functional output.

Here, we investigated the hypothesis that Gγ subunit N-termini undergo combinatorial regulatory phosphorylation. Using the canonical yeast Gγ subunit Ste18 as a model, we measured the sensitivity of N-terminal phospho-acceptor sites Thr^2 (T2), Ser^3 (S3), and Ser^7 (S7) to various stimuli, including GPCR activation by yeast mating pheromone, osmotic stress, glucose stress, and acid stress. Of these three sites, we found that S7 was phosphorylated in response to pheromone-induced GPCR activation and osmotic stress, whereas S3 was phosphorylated in a quantitative manner that was indicative of intracellular pH. We found that phosphorylation at S3 and S7 was interdependent in vivo and that different phosphorylation states had differences in IDR structure and distinct functional effects on GPCR-dependent MAPK activation. Together, these data place G protein γ subunits in the group of proteins governed by combinatorial PTM-regulated IDRs.

Results

The N-terminal IDR of Ste18 undergoes stimulus- and site-specific phosphorylation

The N-terminal IDR of Ste18, $Ste18^{Nt}$, undergoes regulatory phosphorylation in response to pheromone-dependent GPCR activation (18), but was originally discovered by largescale phosphoproteomics analysis of yeast undergoing osmotic stress (23). Considering its regulatory role in the pheromone response pathway, we hypothesized that the tail was a hotspot for phosphorylation-dependent pathway crosstalk. To test this hypothesis, we utilized a phosphorylation-dependent electrophoretic mobility shift assay optimized for Ste18 to measure phosphorylation in response to common cellular stressors known to crosstalk with the pheromone pathway: osmotic stress, nutrient or glucose stress, and pH stress (24). Previously, pheromone-dependent phosphorylation was shown to correspond to the upper (slower-migrating form) of two Ste18-specific bands on immunoblots that

was sensitive to phosphatase (18). We first confirmed this result, showing that Ste18 phosphorylation occurred rapidly in the presence of the α-factor (α-F) mating pheromone and persisted throughout the exposure period of 90 min (Fig. 1A). Next, we exposed cells to osmotic shock with 0.75M potassium chloride, which temporarily activates the osmotic stress pathway within 15 min (25). Ste18 phosphorylation was again evident although different from the pheromone response, occurring to a lesser extent and for a much shorter time, ranging from 15 to 45 min and then decreasing (Fig. 1B). The response was also found to be independent of HOG pathway kinases (fig. S1). In both pheromone and osmotic stress conditions, we also noticed a variable degree of basal phosphorylation in untreated cells (t=0), suggesting that there was a low level of constitutive phosphorylation that occurred in the absence of stimulus or stress (Fig. 1, A and B).

Unlike with pheromone stimulation or osmotic stress, we observed a distinct banding pattern that we had not seen previously in cells rapidly shifted from normal 2% glucose to low-glucose medium (0.00625%), whereby a distinct band (middle band) between the bands corresponding to the phosphorylated and nonphosphorylated proteins appeared shortly after the onset of the stress (0.5 min) (Fig. 1C). This pattern was only observed under low-glucose shock, and did not occur when cells were transferred to media completely lacking glucose, consistent with a previous report that low glucose, but not the absence of glucose, stimulates the phosphorylation of some G proteins (26). Similar to osmotic stress, we found that glucose stress response pathway kinases were not required for this phosphorylation (fig. S2).

Considering that glucose deprivation results in acidification of the intracellular environment and it is this factor that drives the phosphorylation of G protein α subunits in yeast (27), we tested whether the three-band pattern in Ste18 immunoblots could be induced by exposure of cells to acetic acid and whether this pattern was the result of phosphorylation. Indeed, we found that treatment of cells with 45 mM acetic acid resulted in the same mobility shifted bands as those observed under glucose stress (Fig. 1D), and that both the upper and middle bands corresponded to phosphorylated forms of the protein that were sensitive to phosphatase treatment (Fig. 1E). Together, these data suggest that Ste18 phosphorylation is activated in response to a wide range of stimuli, including both GPCR-dependent and independent signals, and, moreover, that phosphorylation occurs at more than one site.

Phosphorylation of Ste18^{Nt} occurs on two distinct phosphosites: S3 and S7

Based on previous mass spectrometry data (23), we hypothesized that phosphorylation would occur on two sites within Ste18^{Nt}, which contains three potential phospho-acceptor residues: T2, S3, and S7 (Fig. 2A). To test this hypothesis, we substituted each acceptor residue in turn with either alanine (phospho-null) or glutamic acid (phospho-mimic) through point mutations introduced into the yeast genomic locus. The resulting mutant yeast strains were exposed to either acetic acid or α-factor mating pheromone and endogenous amounts of Ste18 proteins were evaluated by electrophoretic mobility analysis. Substituting T2 with either alanine (T2A) or glutamic acid (T2E) had no effect on the electrophoretic mobility of Ste18 in either condition, suggesting that it was not a site of phosphorylation under these conditions (Fig. 2, B and C). Under acid stress, in which both the middle and upper bands can be simultaneously detected, alanine substitution of S3 (S3A) resulted in a complete loss

of the middle band, whereas alanine substitution of S7 (S7A) resulted in a complete loss of the upper band (Fig. 2B). Furthermore, nullifying phosphorylation at both S3 and S7 eliminated all phosphorylation-dependent mobility shifts (fig. S3). These results confirmed the identity of the middle band as corresponding to phospho-Ser^3 (pS3) and the upper band as corresponding to phospho-Ser^7 (pS7). These assignments were further confirmed by glutamate substitution of either site (S3E or S7E), which slowed the mobility of the nonphosphorylated lower band (np) in a manner reflective of the relative differences in electrophoretic mobility of pS3 and pS7 bands, respectively (Fig. 2B). Consistent with these assignments, we found that detection of the upper band (corresponding to pS7) in response to pheromone stimulation was completely lost for cells expressing $Ste18^{S7A}$ and was mimicked by the S7E mutation (Fig. 2C). Together, these data show that the electrophoretic mobility of Ste18 reflects the phosphorylation state of two distinct residues in $Ste18^{Nt}$: S3, a pH- and glucose-sensitive phosphosite; and S7, a pheromone- and osmotic stress–sensitive phosphosite.

$Ste18^{pS3}$ and $Ste18^{pS7}$ are inversely regulated in response to intracellular acidification

The characteristics of the acid stress–dependent phosphorylation of $Ste18^{S3}$ are unknown. We hypothesized that changes in the phosphorylation of $Ste18^{Nt}$ in response to acid stress were the direct result of changes in intracellular pH (pH_i), which should manifest as a kinetic and concentration-dependent correlation between pS3 and extracellular acid stress. To test this hypothesis, we monitored changes in the phosphorylation of $Ste18^{Nt}$ relative to changes in pH_i across time and concentration of extracellular acetic acid (Fig. 3). Intracellular pH was monitored through the plasmid-borne expression of pHluorin, a pH-sensitive green fluorescent protein for which the ratio of fluorescence emission in response to excitation at 395 and 480 nm provides a direct readout of the pH environment inside the cytoplasm of the cells (28, 29). Under nonbuffered conditions, in which acetic acid was added directly to cell culture medium without the addition of a buffer, we observed an instantaneous drop in pH_i from pH 7.2 to pH 4.5, which did not recover over the remainder of the 90-min experiment (Fig. 3A). Concomitantly, $Ste18^{pS3}$ abundance increased from 0 to ~20% of the total protein amount with ~15 min ($t_{1/2} < 5$ min) and remained stable for the remainder of the experiment (Fig. 3, C and E). We also observed that $Ste18^{pS7}$ abundance decreased with nearly identical kinetics over the same time (identical $t_{1/2}$), decreasing from ~30% to ~5% of the total Ste18 abundance. Beyond 1 hour, no further changes in phosphorylation were observed, consistent with the highly stable pH_i observed in these cells.

The addition of a buffer to yeast cell culture medium supports the inherent ability of yeast cells to restore pH_i after encountering extracellular acid stress, mediated by the proton pump Pma1 (27). Exploiting this feature of yeast, we next asked whether under buffered conditions, the phosphorylation status of Ste18 would be restored after the cells adapted to pH stress, which would indicate that the phosphorylation state was regulated by pH_i, rather than acetic acid specifically. Consistent with previous observations (27), the addition of acetic acid to give a final concentration of 45 mM in the presence of a buffer had much less of an effect on pH_i, resulting in an instantaneous drop from pH ~7.2 to 6.0, which was followed by an hour-long adaptation period during which pH_i was restored back to the level observed in control cells (Fig. 3B). Concomitant with the kinetics and amplitude

of the changes in pH_i, phosphorylation of S3 was diminished when compared to that in the unbuffered experiment, with $Ste18^{pS3}$ abundance increasing from 0 to only 7% of total protein within 5 min and then decreasing back to an undetectable amount within 60 min (Fig. 3, D and E). As we had observed in the unbuffered experiments, the response of pS7 mirrored that of pS3, with $Ste18^{pS7}$ decreasing from 40 to 20% of total Ste18 abundance by 30 min and then recovering to its original abundance by 90 min. These results demonstrate that $Ste18^{Nt}$ undergoes dynamic, multisite phosphorylation events that are coordinated in response to fluctuations in pH_i.

Considering that $Ste18^{Nt}$ phosphorylation was coordinated with fluctuations in pH_i observed under buffered stress conditions, we asked whether it might serve as a quantitative indicator of the intracellular effects of acid stress. To test this hypothesis, we directly compared the fluorometric response of pHluorin with S3 phosphorylation across a range of acetic acid concentrations added to yeast cell cultures without buffer. Indeed, we found that $Ste18^{pS3}$ abundance exhibited a sigmoidal dose response to increasing concentrations of acetic acid (Hill slope = 5.924), indicating that $Ste18^{Nt}$ was cooperatively sensitive to pH_i (Fig. 4). The pHluorin fluorescence response confirmed the decrease in pH_i with increasing acetic acid concentration but became saturated at 40 mM, above which only the phosphorylation percentage of pS3 was indicative of changing pH_i. We conclude that $Ste18^{pS3}$ is a quantitative indicator of pH_i.

Acid stress–dependent phosphorylation of $Ste18^{S3}$ is affected by multiple kinases

To identify the kinases necessary for acid stress–dependent S3 phosphorylation, we screened 151 different yeast kinase gene deletion strains that included 108 nonessential genes (deletion strains) and 17 essential genes (under the control of a Tet-off promoter), as well as 26 multigene mutants generated specifically to eliminate kinase redundancy when possible (see Materials and Methods). Unexpectedly, S3 phosphorylation was never completely abolished in any strain, but exhibited a wide range of responses across the gene deletion strains in comparison to the response of the wild-type (WT) strain (Fig. 5A, fig. S4, table S1). From this screen, two strains were clear outliers: *vps15Δ* and *pkc1Δ*, in which $Ste18^{pS3}$ was reduced by ~50% compared to that in WT cells as determined through several biological replicates for each case (*vps15Δ*, n = 10; *pkc1Δ*, n = 10) (Fig. 5, B and C). In comparison, $Ste18^{pS7}$ was unaltered in either strain.

Adaptation of yeast to acid stress proceeds through the cell wall integrity (CWI) pathway, which is controlled by the kinase Pkc1 (30). In response to mechanical stress, Pkc1 phosphorylates Ste5 within the RING domain, which mediates the interaction of this scaffold protein with Ste4 and Ste18 (31). Although $Ste18^{S3}$ is not contained within a Pkc1 consensus sequence (32), we hypothesized that other downstream kinases in the CWI might potentially phosphorylate Ste18 in response to acid stress. We tested this by measuring acid stress–dependent S3 phosphorylation in CWI kinase gene deletion strains. However, we found that pS3 was unaffected in cells lacking genes for kinases downstream of Pkc1, including *BCK1*, *MKK1/MKK2*, and *SLT2* (Fig. 5, D to F). Loss of Slt2 phosphorylation in the *pkc1Δ* and CWI kinase deletion strains further confirmed inactivation of the CWI pathway, suggesting that maximal S3 phosphorylation requires

Pkc1, but not the downstream kinases of the CWI pathway (Fig. 5E). Together, these results imply that maximal acid stress–dependent phosphorylation of S3 is partially dependent on the CWI-pathway kinase, Pkc1, as well as other non-CWI kinase(s), including Vps15.

Ste18^{pS3} and Ste18^{pS7} are interactive

Intraprotein PTM interactions, in which the modification of one site in a protein affects the modification of another (often nearby) modification site in the same protein, are common in well-characterized regulatory IDRs (8, 33–36). We assessed the potential for a pS3-pS7 interaction by monitoring the behavior of both sites in response to isolated versus sequential stimulation by pheromone (pS7-activating) or acetic acid (pS3-activating). As shown earlier, we observed a rapid increase in Ste18^{pS7} abundance upon pheromone stimulation that was sustained up to 60 min (Fig. 6A and fig. S5). However, if the cells were pre-treated with the counter-stimulus (acetic acid in the case of pS7) for 15 min, the increase in Ste18^{pS7} abundance was completely inhibited. Moreover, Ste18^{pS7} abundance underwent a rapid and substantial decline upon post-treatment with the counter-stimulus. In comparison, acid-induced Ste18^{pS3} abundance was slightly diminished by pre-treatment with the counter-stimulus (pheromone in the case of pS3), but unlike that of Ste18^{pS7}, was only mildly affected by post-treatment with the counter-stimulus (Fig. 6B and fig. S5).

Whereas the results of the co-stimulation experiments suggested an interaction between pS3 and pS7, the treatment of cells with two stimuli affects many proteins, making it difficult to evaluate the interaction between pS3 and pS7 directly. Therefore, to investigate whether pS3 and pS7 were directly interactive, we quantified phosphorylation at each site in the presence and absence of phospho-nullifying or -mimicking mutations at the neighboring site. We found that the S3A mutation had no effect on the phosphorylation of S7 in response to either pheromone stimulation or acid stress (Fig. 6, C and D, and fig. S6). In contrast, the S3E mutation significantly dampened both pheromone-dependent and acid stress–dependent phosphorylation at S7 by >50% compared to that in WT cells (Fig. 6, E and F, and fig. S6). This effect on S7 phosphorylation was uniform across all time points within each condition, suggesting that the efficiency, but not the dynamics of S7 phosphorylation, were sensitive to phosphorylation at S3. Together with the data from co-stimulation experiments, these results suggest that acid-dependent phosphorylation at S3 is likely to negatively affect pheromone-dependent phosphorylation at S7.

Reciprocal testing of the effects of S7 mutations on S3 phosphorylation further revealed that pS3 and pS7 were differentially sensitive to mutation at the neighboring phosphosite. S3 phosphorylation was not observed in pheromone-treated S7A or S7E mutant cells (Fig. 6, G and I and fig. S6), but did show a three-fold increase from ~6 to ~18% in response to acid stress in S7A cells (Fig. 6H, and fig. S6), suggesting the phosphorylation of S7 would negatively impact phosphorylation at S3. This was confirmed in S7E cells, in which acid-dependent phosphorylation of S3 was diminished by ~two-fold relative to that in S7A cells (compare Fig. 6, H and J, red traces), despite being slightly higher than the extent of phosphorylation observed in WT cells (Fig. 6J, red vs. gray). Together, these data provide evidence of a negative interaction between pS3 and pS7 in Ste18, whereby phosphorylation on one site dampens phosphorylation on the other site.

Phosphorylation alters the structure of Ste18^{Nt} in vitro

Evidence indicates that multisite phosphorylation in an IDR can in some cases produce intrinsic disorder-to-order transitions (37–39). To assess this possibility for Gγ subunit N-terminal IDRs, we analyzed the effects of site-specific phosphorylation on the structure of the Ste18 N-terminus (residues 1 to 13) by molecular dynamics (MD) simulations coupled with circular dichroism (CD) spectroscopy. MD analysis of each 13-mer peptide isoform suggested a tendency for the IDR to adopt an α-helical structure in the vicinity of the phosphosite, occurring near the extreme N-terminus when S3 was phosphorylated and further C-terminal when S7 was phosphorylated (Fig. 7, A and B, and fig. S7). The secondary structure propensities of the fully phosphorylated (pS3pS7) and nonphosphorylated (NP) peptides were considerably lower in comparison (Fig. 7, C and D, and fig. S7). Whereas it was at first surprising that the fully phosphorylated form mimicked the nonphosphorylated form, a time-resolved snapshot for this peptide provided evidence that metal ions may bridge the two phosphate groups and prevent helical structure formation within the tail (Fig. 7C, inset).

The general trends observed by MD simulation were corroborated by differential CD spectropolarimetry of synthetic phosphopeptides. First, a random coil was the dominant feature of each peptide regardless of phosphorylation state and consistent with the prominence of this characteristic across all MD simulations (Fig. 7E, and fig. S7). Second, the pS3 and pS7 peptides produced the largest spectral differences with the greatest overlap, displaying more secondary structural character relative to the nonphosphorylated form (Fig. 7F, and fig. S7). Third, the doubly phosphorylated peptide (pS3pS7) produced the least prominent difference spectrum relative to the nonphosphorylated peptide (Fig. 7F) and consistent with the relative rarity of α or β secondary structural character in the MD simulation of these peptides (Fig. 7, C and D). We conclude that the N-terminal IDR of Ste18 is innately intrinsically disordered and that site-specific, but not combined, phosphorylation, promotes weak but detectable secondary structure within this region.

Combinatorial phosphorylation on Ste18^{Nt} tunes MAPK activation in vivo

Combinatorial protein modification is defined in one sense by the occurrence of distinct spatial combinations of protein modification that yield distinct functional outcomes (8). Phosphorylation of Ste18^{Nt} controls Fus3 activation rate and amplitude. Phospho-nullifying mutations enhance the activation rate and amplitude of Fus3, whereas phosphomimic mutations have the opposite effect (18). Moreover, these effects of the Gγ tail become further exaggerated in the presence of Ste5ND (18), which is a docking mutant of the Gβγ effector Ste5 that prevents its binding to, and regulation by, Fus3 (40). Therefore, we used Fus3 activation kinetics in cells expressing Ste5^{WT} or Ste5ND to report on the functional effect of combinatorial phosphorylation in Ste18^{Nt}. Because pheromone does not induce S3 phosphorylation, we combined glutamate substitutions at position 3 (S3E) to mimic the effects of acid-induced S3 phosphorylation with alanine substitutions at position 7 to nullify naturally occurring S7 phosphorylation inherent to the pheromone response, resulting in four distinct protein isoforms: Ser^{3}/Ser^{7} (S3/S7) (WT), S3/A7, E3/S7, and E3/A7. This approach minimized the potential for over-engineering the protein so as to capture realistic effects of combinatorial phosphorylation (that is, serine rather than alanine is maintained as the

natural residue for position); and also circumvented the treatment of cells with acetic acid, which broadly affects many proteins in addition to Ste18 that could preclude any ability to decipher Ste18-specific effects on G protein signaling. Each Gγ isoform was expressed endogenously in either $Ste5^{WT}$ or $Ste5^{ND}$ cells, which were then stimulated with pheromone and monitored for Ste18 phosphorylation and MAPK activation (Fig. 8, A to F, and fig. S8). We found that pheromone-induced S7 phosphorylation was identical between $Ste5^{WT}$ and $Ste5^{ND}$ cells, confirming that disruption of the Fus3 regulatory site on Ste5 has no effect on Ste18 phosphorylation at S7, and consistent with previously reported data (18). Similarly, we found no difference in the S3E-dependent inhibition of S7 phosphorylation between the $Ste5^{WT}$ and $Ste5^{ND}$ strains (Fig. 8, A and B, and fig. S8).

Next, we compared the activation of the pheromone-responsive MAPKs in each strain. Activation of the yeast mating pathway stimulates phosphorylation of Fus3 and also Kss1, which can both be monitored simultaneously. Overall, Kss1 activation was relatively unaffected by Ste18 phosphosite mutants in either the $Ste5^{WT}$ or $Ste5^{ND}$ background, despite the large increase in its overall activation in $Ste5^{ND}$ cells (Fig. 8, C and D, and fig. S8), which was documented previously (41). In contrast, we found that Fus3 activation kinetics were dependent on the phosphorylation state of Ste18. In $Ste5^{WT}$ cells, Fus3 activation was sensitive to the S7A mutation, resulting in faster peak activation that occurred at 15 min rather than at the typical 30-min peak in $Ste5^{WT}$ cells (Fig. 8E, and fig. S8). In $Ste5^{ND}$ cells, Fus3 activation was more pronounced and revealed functional distinctions between the different Ste18 phosphosite mutants. $Ste5^{ND}$ cells expressing WT Ste18 (S3/S7) produced a characteristic peak of Fus3 activation at 30 min, but with ~2.5-fold greater total signal than occurred for $Ste5^{WT}$ cells (Fig. 8F). S7A (that is, S3/A7), which prevented all phosphorylation in response to pheromone, did not change Fus3 activation intensity but shortened peak activation time two-fold to 15 min. In contrast, E3/S7, which models a form of Ste18 that is maximally phosphorylated at both S3 and S7, repressed Fus3 activation without altering the rate of peak activation in the $Ste5^{ND}$ background. Lastly, we analyzed E3/A7, which models a form of Ste18 that is only phosphorylated at position 3 but not at position 7 (Fig. 8F). Cells expressing this form of Ste18 exhibited WT (S3/S7) behavior when combined with $Ste5^{ND}$. Together, these data suggest that phosphorylation in the N-terminal IDR of a G γ subunit, and in Ste18 specifically, can have distinct structural and functional effects that govern G protein signaling outcomes.

Discussion

We have presented here evidence that the intrinsically disordered N-terminal tails of G γ subunits can undergo stimulus-dependent, combinatorial, multisite phosphorylation events that alter their inherent structure and function. We characterized in detail the site-specific N-terminal phosphorylation of Ste18, the single canonical Gγ subunit required for pheromone-dependent G protein signaling in yeast. Our results showed that $Ste18^{Nt}$ was differentially phosphorylated at two distinct serine residues, S3 and S7, in response to a range of stimuli, including pheromone-dependent GPCR activation, osmotic stress, glucose stress, and pH stress. Phosphorylation of S3 in particular was sensitive to pH stress and promoted a state in which both sites were phosphorylated simultaneously. We exploited this fact to test the hypothesis that Gγ subunits are among the short list of proteins, such as histones and

GPCRs, that undergo functional combinatorial modification within their terminal IDRs. Through a combination of in vivo and in vitro approaches, we provided several pieces of evidence in support of this hypothesis. We showed: (i) that phosphorylation between S3 and S7 is likely interactive such that phosphomimicry at one site inhibits phosphorylation on the other site; (ii) that phosphorylation induced detectable structural changes in the N-terminal IDR in vitro; (iii) that the structural effects of single- versus double-site phosphorylation were distinct; and (iv), that different patterns of phospho-mimicry or phosphorylation on S3 and S7 result in distinct MAPK activation profiles in vivo. Together, these data support the hypothesis that Gγ N-terminal IDRs are multi-conditional targets of cell stress–mediated combinatorial phosphorylation that govern G protein signaling.

Phosphorylation, not structural change, likely dominates the regulatory effects of Ste18^{Nt}

The functional effect of any PTM can be mediated through two possibilities. A modification may elicit a change in structure, and this structural change alters protein function (through altered tertiary or quaternary protein structure). Alternatively, a modification may itself disrupt or promote function by generating a new surface with which proteins may interact or by disrupting an existing surface that is necessary for interaction. IDRs are inherently disordered, and, as such, their modification is often suspected to mediate functional effects through the second of these two options. However, emerging evidence suggests that PTMs on IDRs can elicit disorder-to-order transitions, such as the formation of phosphorylation-stabilized β-sheets (39). Here, we investigated the structural effects of phosphorylation on an N-terminal IDR within a canonical Gγ subunit. Our results suggest that, despite some minor changes in observable secondary structure, the intrinsic disorder of these regions largely persists regardless of phosphorylation state (Fig. 7). Consequently, we did not find a strong correspondence between the structural and functional effects of phosphorylation in the Ste18^{Nt} (compare Fig. 7 and Fig. 8). Therefore, our data suggest that phosphorylation, more so than the structural changes induced by phosphorylation, mediate the regulatory properties of Gγ N-terminal tails.

Multiple phosphosites in Ste18^{Nt} relay crosstalk from a range of cellular stress pathways

Previous work showed that pheromone- and MAPK-dependent feedback phosphorylation of Ste18^{Nt} inhibits Ste5-dependent plasma membrane association and phospho-activation of Fus3 phosphorylation (18). Our work extends these findings to show that Ste18^{Nt} phosphorylation occurs at multiple sites and in response to various cellular stress stimuli, including osmotic, glucose, and pH-dependent stresses. This discovery is consistent with the role of Ste18^{Nt} phosphorylation as a negative regulator of MAPK signaling and suggests that in yeast, phosphorylation of the Gγ subunit is one of many ways in which negative feedback can be relayed to the mating response. Indeed, we confirmed that under hyperactivating conditions facilitated by mutations in the Gβγ effector Ste5, activation of the primary mating-specific MAPK Fus3 occurred unhindered in the absence of Ste18^{Nt} phosphorylation, was partially repressed in response to single-site phosphorylation alone, and was maximally repressed in response to dual-site phosphorylation (Fig. 8F). Because S3 and S7 phosphorylation events were distinct in their conditional dependence (whereas S3 phosphorylation was responsive to low glucose or acid stress, S7 phosphorylation was responsive to pheromone stimulation or osmotic stress), it suggests that they function like

cellular stress indicators that relay crosstalk from different stress pathways and broaden the capacity of Gβγ-dependent signaling to be modulated in response. Furthermore, phosphorylation was dynamic and responsive, whereby it was maintained only for the duration of the stress or until the cell hed equilibrated to the stress, which can be seen in the short pulse of S7 phosphorylation observed under osmotic stress (Fig. 1B), the extended response to acid stress (Fig. 3C), the temporary response to acid in buffered culture medium (Fig. 3D), and the rapid decline in S7 phosphorylation in pheromone-stimulated cells that were suddenly exposed to acid stress (Fig. 6A).

Although our data provide evidence that such crosstalk can determine G protein signaling through Gβγ subunits, new questions also arise from this work. For example, the stoichiometry of Ste18 phosphorylation in response to cellular stress (5 to 20%) is rather low compared to the extent of phosphorylation observed in response to pheromone (~80%), which could suggest that $Ste18^{Nt}$ may not be a primary or ideal target for kinases activated under the stresses tested here, that there are strict cellular localization constraints for crosstalk to occur efficiently under each stress, or that we have gleaned the potential for stress crosstalk through $Ste18^{Nt}$ but have not yet identified the linchpin stressor or stress condition that would promote high stoichiometry phosphorylation and regulation. Indeed, our first glimpse into Ste18 phosphorylation came from studies of osmotic stress, only to find later that pheromone-dependent phosphorylation was more predominant (18). Further work will be necessary to determine the answers to these questions and to evaluate the physiological relevance of these molecular discoveries in a cellular context, wherein Gγ regulation is but one of thousands of proteome-wide targets of extracellular stress.

Multiple conditions, multiple sites, multiple kinases

The kinases that phosphorylate S3 and S7 in $Ste18^{Nt}$ are different, due not only to the distinctness of each site in the protein, but also to the conditions under which they become phosphorylated. Previous evidence suggests that Fus3 is responsible for phosphorylation of S7 in response to pheromone-dependent GPCR activation (18). However, the fact that Fus3 is not activated by osmotic stress indicates that other S7 kinases must also exist. The high osmolarity glycerol (HOG) pathway is essential for yeast adaptation to hyperosmotic stress (42). We evaluated S7 phosphorylation in HOG pathway kinase gene deletion strains. Unexpectedly, osmotic stress–induced S7 phosphorylation was not driven by the main MAPK of the HOG pathway, Hog1, or any other upstream kinases in the pathway (fig. S1). Furthermore, the observation of basal phosphorylation suggests the involvement of a third S7 kinase. Thus, beyond the fact that multiple phosphosites exist in $Ste18^{Nt}$, condition-specific phosphorylation patterns suggest that a site can be targeted by multiple kinases relaying crosstalk through the same residue.

In contrast to S7, S3 does not fit within a well-defined kinase consensus sequence and is difficult to predict by sequence alone (43). We detected S3 phosphorylation in response to both glucose deprivation and acid stress, although the effect was very minor under glucose stress (Fig. 1). The kinase Snf1, which is homolog of AMP-activated protein kinase (AMPK) in mammals, is essential for mediating glucose repression signaling in response to glucose deprivation, and three upstream kinases, Tos3, Elm1, and Sak1, are required

for Snf1 phosphorylation and activation (44). Glucose deprivation induces phosphorylation of the G protein α subunit Gpa1, which is mediated by all three of the Snf1-activating kinases (26). In contrast, we did not observe any change in S3 phosphorylation upon glucose starvation of *snf1Δ* cells and saw only a minor decrease in S3 phosphorylation in response to glucose deprivation of *tos3Δ elm1Δ sak1Δ* triple deletion cells (fig. S2). In contrast, we found two kinases, Vps15 and Pkc1 that appeared to be necessary to maximize acid stress–dependent S3 phosphorylation. Vps15 is a serine and threonine kinase essential for the activation and localization of the phosphatidylinositol 3-kinase Vps34 to subcellular plasma membranes (45). Vps15 and Vps34 form a complex that mediates a number of intracellular signaling events, including vacuolar protein sorting (46), TORC1 activation in response to glutamine stress (47), autophagy (48), V-ATPase activity (49), and the pheromone response (50). Despite the involvement of Vps15 in several environmental stresses, we were unable to find prior evidence of acid stress–dependent regulation of Vps15 kinase activity in yeast, nor a well-defined consensus sequence that would otherwise provide additional support for its potential role as a Gγ kinase. Thus, our data do not exclude the possibility that Vps15 functions indirectly to affect Ste18 phosphorylation.

In contrast to Vps15, Pkc1 and the CWI pathway are activated by pH stress (30). We found from experiments with deletion strains that Pkc1, but not other downstream CWI kinases, was necessary for maximal phosphorylation of $Ste18^{S3}$ in response to acidic pHi stress (Fig. 5, E and F) The consensus sequence for Pkc1 phosphosites, generated by hundreds of different substrates (32), suggests that S3 is not a direct target of the kinase, but rather another kinase whose action on Ste18 is Pkc1-dependent (Fig. 5D). Considering the breadth of our survey across 151 different kinase gene mutants, identifying the acid stress–dependent kinases(s) sufficient for $Ste18^{S3}$ phosphorylation remains an ongoing challenge and suggests the possibility of kinase redundancy for this phosphosite. In any case, we showed that S3 phosphorylation functions as a quantitative indicator of intracellular pH (Fig. 4), and, in view of the fact that the complete CWI pathway is not essential for this effect, this suggests that activation of the responsible kinase may depend on proton second-messaging. Indeed, emerging evidence that protons can function as second messengers in G protein signaling pathways (27, 51, 52) provides support for this hypothesis.

Interdependence of Gγ phosphorylation and Gβγ effectors

Whereas we showed the physiological relevance of Ste18 phosphorylation in yeast, it was also not completely independent of the Gβγ effector Ste5. Indeed, we confirmed that the effects of Gγ phosphorylation were most prominent when coupled with the Fus3 nondocking mutant of Ste5 ($Ste5^{ND}$), which cannot be phospho-regulated by Fus3 (Fig. 8F). Indeed, previous work showed that genetic mutations in $Ste18^{Nt}$ and Ste5 synergize to control MAPK signaling (18). Pkc1 phosphorylates Ste5 within the $Ste5^{RING}$ domain, which mediates the interaction of this scaffold protein with Ste4 and Ste18 (31). Thus, co-regulation of both Gβγ subunits and their effectors may play complementary roles in the modulation of Gβγ signaling. In yeast, additional Ste4 and Ste18 effectors (Far1, Ste20, and Cdc24) are also key players in the Gβγ-dependent pheromone response. Whether they, like Ste5, synergize with phosphorylated Ste18 remains unknown. In humans there are 5 Gβ and 12 Gγ subunits, which can form a range of Gβγ dimers that interact directly with several

different effectors (53). Many of these Gγ subunits are phosphorylated in their N-terminal IDRs (19, 54), but they have not been studied to elucidate the functional importance of these sites, especially in terms of their dependence on effector modification state. Thus, continued work in this area can expand the existing paradigm of Gβγ signaling not only in yeast but also in other organisms for which there is growing evidence to support the hypothesis that N-terminal IDRs of Gγ subunits are combinatorially regulated governors of G protein signaling.

Materials and Methods

Yeast strains and plasmids

Unless specified otherwise, all strains used in this study were derived from the *BY4741* (*MATa leu2Δ met15Δ his3Δ ura3Δ*) background (see table S2). All mutants were constructed by delitto perfetto mutagenesis (55) and verified by PCR amplification and dideoxy sequencing (Eurofins MWG Operon). Cells lacking *PKC1* (*pkc1*Δ; *DL376*) and the isogenic WT strain (*DL100(1783)*) (56) were graciously provided by Dr. David Levin (Boston University). Temperature-sensitive *PKH1/2* (*pkh1*^{D398G} *pkh2*Δ; *INA106–3B*) and the isogenic WT strains (*15Dau*) were graciously provided by Dr. Kunihiro Matsumoto (Nagoya University) (57). Temperature-sensitive *YCK1/2* (*yck1*-Δ1 *yck2–2*^{ts}; *LRB345*) and the isogenic WT strain (*LRB341*) were graciously provided by Dr. Lucy Robinson (LSU) (58). To construct *pRS313*- and *pRS316-HA-STE18*, the primers ZNT433 (5’TGGAGCTCCACCGCGGTGGCGGCCGCTAGGGCGCGACACGTCTAAA3’) and ZNT434 (5’TCGAATTCCTGCAGCCCGGGGGATCCCAGCGAGATTTATTTCGAAA3’) were used to amplify WT *HA-STE18* including its endogenous promoter (−510bp) and terminator (+467bp) from the *YMT235* strain genome. The PCR product was subcloned into the pRS313 or pRS316 plasmids digested with *NotI* and *BamHI* restriction sites using the sequence and ligation independent cloning (SLIC) method (59). The plasmid used for screening HOG pathway kinase deletion strains, pRS316-CUP1-HA-STE18, was graciously provided by Dr. Tatiana Chernova.

Media and growth conditions

Depending on the treatment conditions, yeast strains were grown in either YPD growth medium (Yeast Extract, Peptone, 2% dextrose media) or synthetic complete (SC) (or SC drop-out) medium with 2% dextrose. When experiments were performed in buffered conditions, SC medium with 2% dextrose was buffered by the addition of 50 mM dibasic potassium phosphate and 50 mM dibasic sodium succinate and adjustment to pH 5.0 by the addition of HCl (27). Cells were grown at 30°C to mid-log phase (OD_{600}: 0.75 to 0.85), which followed by treatment appropriate for the specific experiment. After the cells were treated for the appropriate time, cell growth was stopped by the addition of 5% trichloroacetic acid (TCA), after which the cells were immediately harvested by centrifugation at 3724*g* in an Allegra X-14R Beckman Coulter Centrifuge at 4°C, washed with ice-cold Milli-Q water, and frozen at −80°C. Specific treatment conditions were as follows. For GPCR activation, cells were treated with α-factor peptide hormone (Genscript) at a final concentration of 3 μM. For osmotic stress, cells were collected by centrifugation and resuspended in the same medium supplemented with 0.75 M KCl for the appropriate

time, as described previously (60). To evaluate Ste18 phosphorylation in HOG pathway kinase deletion strains, expression of HA-STE18 was induced by 100 μM copper sulfate in BY4741 cells harboring the pRS316-CUP1-HA-STE18 plasmid at an OD_{600} of 0.2. As cells reached mid-log phase, osmotic stress was induced as described earlier. For glucose stress, cells were collected by centrifugation, washed with the same medium lacking glucose, and re-suspended in glucose-free synthetic medium supplemented with the desired amount of glucose for the appropriate time (27). To evaluate Ste18 phosphorylation in *snf1Δ* and *tos3Δ elm1Δ sak1Δ* triple deletion cells, cells were transformed with the pRS316-HA-STE18 plasmid and glucose stress was induced as described earlier. For acetic acid stress, cells were grown in buffered or unbuffered SC medium containing 2% dextrose, which was followed by the addition of acetic acid to a final concentration fo 45 mM unless otherwise noted (27). For costimulations, cells were grown in unbuffered SC medium. Before treating cells with either 3 μM α-factor or 45 mM acetic acid, the cells were pretreated with 45 mM acetic acid (for 15 min) or 3 μM α-factor (for 5 min), respectively.

Cell lysis and Western blotting analysis

Cell pellets were subjected to glass bead lysis in the presence of TCA buffer according to the standardized protocol described previously (61). The protein concentration was measured with a DC Protein Assay (Bio-Rad). Protein extracts were separated by SDS-PAGE with either 7.5 or 12.5% acrylamide. Primary antibodies and dilutions used for immunoblotting included: phosphorylated Slt2, Kss1, and Fus3 (Phospho-p44/42 MAPK, Cell Signaling Technologies, Cat #9101; 1:500); hemagglutinin antigen epitope (HA, Cell Signaling Technologies, Cat #3724; 1:3000); total Slt2 (Mpk1 antibody D-1, Santa Cruz Biotech Cat#374434; 1:1000); phosphorylated Snf1 [Phospho-AMPKα (Thr^{172}) (D79.5E), Cell Signaling Technology, Cat #4188; 1:2000); glucose-6-phosphate dehydrogenase (loading control; LC) (Sigma-Aldrich, Cat #A9521; 1:50,000). In all cases, a horseradish peroxidase (HRP)-conjugated secondary antibody (goat-anti-rabbit) (Bio-Rad, Cat # 1705046; 1:5000) was used for detection. The signal was detected with enhanced chemiluminescence (ECL) reagent (PerkinElmer catalog #NEL 104001EA) and developed on film E3018 HyBlot CL Autoradiography Film (Denville Scientific). In all cases, several exposures were made and only those exposures for which all signals were below saturation were used for quantification. Quantification was achieved by hi-resolution scanning of appropriate films followed by image densitometry with ImageJ software to quantify signal intensities (62).

Analysis of Ste18 phosphorylation in yeast kinase mutant strains in response to acid stress

A total of 151 strains were screened for the kinases responsible for Ste18^{S3} phosphorylation under acetic acid stress, including 108 nonessential kinases (deletion strains from the yeast open reading frame knockouts by the Saccharomyces Genome Deletion Project), 17 essential kinases (TET-titratable promoter strains from the Hughes Laboratory), 24 multideletion strains, and two temperature-sensitive strains (table S3). Analysis of Ste18 phosphorylation in the mutant strains was accomplished by transformation of each strain with either pRS316-HA-STE18 or pRS313-HA-STE18. For single and multiple deletion strains, cells were then grown in SC-URA or SC-HIS medium and treated with acetic acid for up to 15 min as described earlier. For the pkc1Δ and mkk1Δ/mkk2Δ strains, the medium

was supplemented with 1 M sorbitol to facilitate growth. For TET-titratable promoter strains, cells were grown in SC-HIS medium until they reached an OD_{600} of 0.8, and then were diluted back to an OD_{600} of 0.003, split, and treated with or without doxycycline (10 μg/ml, Sigma). Cells were then grown to mid-log phase and treated with acetic acid as described earlier. For *yck*^{ts} strains, cells were grown at 24°C to an OD_{600} of 0.8 and then each culture was split into two parts: one was subjected to acetic acid treatment and the other was incubated at 37°C for 30 min before undergoing acetic acid treatment. For *pkh*^{ts} strains, cells were grown at 24°C to an OD_{600} of 0.8 and then each culture was split into two parts: one was subjected to acetic acid treatment and the other was incubated at 37°C for 60 min before undergoing acetic acid treatment. Each transformed strain was grown in one copy or multiple replicates (biological replicates) and analyzed by Western blotting with respect to the isogenic WT strain on the same blot. For Tet-off strains, the doxycycline-treated mutant was analyzed with respect to the untreated mutant. Ste18 phosphorylation percentages calculated from both biological and analytical replicates (rerun of the same sample) were included in the quantitative analysis.

Phosphatase assay

Cells were grown as described earlier in a nonbuffered synthetic medium and treated with 45 mM acetic acid for 15 min, which was followed by the addition of TCA, cell harvesting by centrifugation, and freezing at −80C. Cells were subjected to glass bead lysis in the presence of 1x phosphatase buffer mix [1x PMP buffer (New England Biolabs), 1x $MnCl_2$, and 1x EDTA-free protease inhibitors (Roche)], as described previously (18). Lysates were clarified by centrifugation and the supernatant was split. One half was treated with lambda protein phosphatase enzyme (New England Biolabs, P0753S) at a final concentration of 2.25 U/μl for 30 min at 30C. The other half was incubated in the same manner in the absence of phosphatase to serve as a control. 6x SDS loading dye was added to all samples, which were then boiled to stop the reaction. The samples were then resolved by SDS-PAGE and subjected to Western blotting analysis.

Measurement of pH_i

For pH_i measurement, yeast cells were transformed with the pZR4.1 plasmid encoding pHluorin under the *TEF1* constitutive promoter (63), and pH_i was measured as described previously (27). To generate the calibration curves (fig. S9), mid-log phase cells expressing pHlourin were permeabilized with digitonin (at a final concentration of 100 μg/ml; Sigma-Aldrich, Cat #D141) for 10 min at 30°C. Permeabilized cells were washed with PBS (25 mM potassium phosphate, 100 mM KCl, pH 7.0) followed by resuspension in PBS ranging from pH 5.0 to pH 8.0 (pH 5, 5.5, 6, 6.5, 7, 7.5, and 8). The ratio of pHluorin emission fluorescence intensity at 520 nm produced by excitation at 395 and 480 nm was measured with a Synergy H1 hybrid fluorescence plate reader (Biotek). For pH_i measurements, Prism software, v8 (GraphPad Software) was used to convert pHluorin fluorescence intensities emitted upon excitation at the two excitation wavelengths to pH values using the calibration curve.

CD spectropolarimetry

Commercial synthetic $Ste18^{Nt}$ peptides were synthesized with N-terminal acetylation and C-terminal amidation, and various combinations of S3 and S7 phosphorylation (or nonphosphorylation) and enriched to 95% purity (Genscript). Lyophilized peptides were reconstituted in deionized water at a concentration of 2.5 mg/ml and further diluted as necessary with 10 mM potassium phosphate buffer (pH 7). Far-ultraviolet (190 to 250 nm) CD spectroscopy was performed on a Jasco J-815 CD spectrometer equipped with a Peltier temperature control unit. Peptide samples were diluted to 0.25 mg/ml in 10 mM potassium phosphate buffer (pH 7). A quartz cuvette with a 1-mm path length was used at 25°C in this experiment. Measurements were performed with a 50 nm/min scan rate in 0.2-nm steps at a 1-s response time and a 1 nm bandwidth. Single CD spectra were averaged over 15 scans after buffer baseline correction.

MD simulations

MD simulations were performed with NAMD2.13 (64) and Amber16 (65). The CHARMM22* protein (66) and CHARMM36 nucleic acid force field (67) were used to describe the peptides, and the TIP3P water model (68) was used to describe the solvent and ions. The initial structure of the Ste18 N-terminus (residues 1 to 13) was prepared with VMD and its plugin, Molefacture (69). All four phosphorylated states of the peptide were constructed, including phosphorylation at Ser^3 (pS3), Ser^7 (pS7), both Ser^3 and Ser^7 (pS3pS7), and nonphosphorylated (NP). Each peptide was placed in a water box, and ions were added to neutralize the system at a concentration of 150 nM NaCl. The final system size was around 20,300 atoms. Each system was equilibrated at 400K and a constant volume for 4 ns to randomize the starting conformation, and then cooled at 298 K and 1 atm for 2 ns. Next, two independent 4-μs production runs were performed for each system at 298 K and constant volume. The temperature was maintained using Langevin dynamics for all simulations, and the pressure was kept at 1 atm using the Langevin piston method when applied (70). The equilibration simulations were performed using a 2-fs time step. Hydrogen mass repartitioning (HMR) was used for the production runs to reach a time step of 4 fs (71, 72). All simulations were performed under periodic boundary conditions with a cutoff at 12 Å for electrostatic and Lennard-Jones interaction and a switching function beginning at 10 Å. Long-range electrostatic interactions were calculated by the particle-mesh Ewald (PME) method (73). System setup, analysis, and visualization were performed with VMD.

Statistical analysis

All statistical analyses were performed with Prism software, v8 (GraphPad Software). Statistical significance was determined by two-way ANOVA with either a Bonferroni or Sidak’s test for post-hoc test for multiple comparisons. X

Supplementary Material

Refer to Web version on PubMed Central for supplementary material.

Acknowledgments:

We thank N. V. Hud (GIT) for CD spectropolarimeter access, A. Reddi (GIT) for the pHluorin plasmid, D. Levin (Boston U.) for the *pkc1*Δ yeast strains, K. Matsumoto (Nagoya U.) for the *pkh-ts* yeast strains, L. Robinson (LSU) for the temperature-sensitive *yck1/2* yeast strains, K. Lobachev (GIT) for the kinase deletion and Tet-off strains, T. Chernova (Emory) for the *pRS316-CUP1-HA-STE18* plasmid, and K. Mukherjee and P. Baradaran-Mashinchi for the Ste18 constructs. Special thanks to D. Isom for critical review and discussion.

Funding: This work was funded in part by National Institutes of Health grants R01-GM117400 to M.T. and R01-GM123169 to J.C.G., and by the Southeast Center for Mathematics and Biology through grants NSF-DMS1764406 and Simons Foundation/SFARI-594594 to M.T. Computational resources were provided through the Extreme Science and Engineering Discovery Environment (XSEDE; TG-MCB130173), which is supported by the NSF Grant Nation. This work also used the Hive cluster, which is supported by the National Science Foundation under grant number 1828187 and is managed by the Partnership for an Advanced Computing Environment (PACE) at the Georgia Institute of Technology.

References and Notes

1. Strahl B, Allis C, The language of covalent histone modifications. Nature. 403, 41–45 (2000). [PubMed: 10638745]
2. Harlen KM, Churchman LS, The code and beyond: transcription regulation by the RNA polymerase II carboxy-terminal domain. Nat. Rev. Mol. Cell Biol. 18, 263–273 (2017). [PubMed: 28248323]
3. Verdier-Pinard P, Pasquier E, Xiao H, Burd B, Villard C, Lafitte D, Miller LM, Angeletti RH, Horwitz SB, Braguer D, Tubulin proteomics: towards breaking the code. Anal. Biochem. 384, 197–206 (2009). [PubMed: 18840397]
4. Nobles KN, Xiao K, Ahn S, Shukla AK, Lam CM, Rajagopal S, Strachan RT, Huang T, Bressler EA, Hara MR, Shenoy SK, Gygi SP, Lefkowitz RJ, Distinct phosphorylation sites on the β(2)-adrenergic receptor establish a barcode that encodes differential functions of β-arrestin. Sci. Signal. 4, ra51 (2011).
5. Yang Z, Yang F, Zhang D, Liu Z, Lin A, Liu C, Xiao P, Yu X, Sun J-P, Phosphorylation of G Protein-Coupled Receptors: From the Barcode Hypothesis to the Flute Model. Mol. Pharmacol. 92, 201–210 (2017). [PubMed: 28246190]
6. Torrecilla I, Tobin AB, Co-ordinated covalent modification of G-protein coupled receptors. Curr. Pharm. Des. 12, 1797–808 (2006). [PubMed: 16712489]
7. Yang X-J, Multisite protein modification and intramolecular signaling. Oncogene. 24, 1653–62 (2005). [PubMed: 15744326]
8. Lothrop AP, Torres MP, Fuchs SM, Deciphering post-translational modification codes. FEBS Lett. 587, 1247–57 (2013). [PubMed: 23402885]
9. Hamm HE, The many faces of G protein signaling. J. Biol. Chem. 273, 669–72 (1998). [PubMed: 9422713]
10. Dohlman HG, Thorner JW, Regulation of G protein-initiated signal transduction in yeast: paradigms and principles. Annu. Rev. Biochem. 70, 703–54 (2001). [PubMed: 11395421]
11. Higgins JB, Casey PJ, In Vitro processing of recombinant G protein γ subunits: Requirements for assembly of an active βγ complex. J. Biol. Chem. 269, 9067–9073 (1994). [PubMed: 8132644]
12. Pronin a N., Gautam N, Proper processing of a G protein gamma subunit depends on complex formation with a beta subunit. FEBS Lett. 328, 89–93 (1993). [PubMed: 8344437]
13. Dingus J, Wells CA, Campbell L, Cleator JH, Robinson K, Hildebrandt JD, G Protein betagamma dimer formation: Gbeta and Ggamma differentially determine efficiency of in vitro dimer formation. Biochemistry. 44, 11882–11890 (2005). [PubMed: 16128590]
14. Dowell SJ, Bishop a L., Dyos SL, Brown a J., Whiteway MS, Mapping of a yeast G protein betagamma signaling interaction. Genetics. 150, 1407–17 (1998). [PubMed: 9832519]
15. Leeuw T, Wu C, Schrag JD, Whiteway M, Thomas DY, Interaction of a G protein beta subunit with a conserved sequence in Ste20/PAK family protein kinases. Nature. 4, 191–195 (1998).
16. Bonacci TM, Ghosh M, Malik S, V Smrcka A, Regulatory interactions between the amino terminus of G-protein betagamma subunits and the catalytic domain of phospholipase Cbeta2. J. Biol. Chem. 280, 10174–81 (2005). [PubMed: 15611108]

17. Brand CS, Sadana R, Malik S, Smrcka AV, Dessauer CW, Adenylyl Cyclase 5 Regulation by Gbetagamma Involves Isoform-Specific Use of Multiple Interaction Sites. Mol. Pharmacol. 88, 758–767 (2015). [PubMed: 26206488]
18. Choudhury S, Baradaran-Mashinchi P, Torres MP, Negative Feedback Phosphorylation of Gγ Subunit Ste18 and the Ste5 Scaffold Synergistically Regulates MAPK Activation in Yeast. Cell Rep. 23, 1504–1515 (2018). [PubMed: 29719261]
19. Dewhurst HM, Choudhury S, Torres MP, Structural Analysis of PTM Hotspots (SAPH-ire)--A Quantitative Informatics Method Enabling the Discovery of Novel Regulatory Elements in Protein Families. Mol. Cell. Proteomics. 14, 2285–97 (2015). [PubMed: 26070665]
20. Chakravorty D, Assmann SM, G protein subunit phosphorylation as a regulatory mechanism in heterotrimeric G protein signaling in mammals, yeast, and plants. Biochem. J. 475, 3331–3357 (2018). [PubMed: 30413679]
21. Yasuda H, Lindorfer MA, Myung CS, Garrison JC, Phosphorylation of the G protein gamma12 subunit regulates effector specificity. J. Biol. Chem. 273, 21958–65 (1998). [PubMed: 9705336]
22. Ueda H, Yamauchi J, Itoh H, Morishita R, Kaziro Y, Kato K, Asano T, Phosphorylation of F-actin-associating G protein gamma12 subunit enhances fibroblast motility. J. Biol. Chem. 274, 12124–8 (1999). [PubMed: 10207039]
23. Soufi B, Kelstrup CD, Stoehr G, Fröhlich F, Walther TC, V Olsen J, Global analysis of the yeast osmotic stress response by quantitative proteomics. Mol. Biosyst. 5, 1337–1346 (2009). [PubMed: 19823750]
24. Saito H, Regulation of cross-talk in yeast MAPK signaling pathways. Curr. Opin. Microbiol. 13, 677–83 (2010). [PubMed: 20880736]
25. Hao N, Zeng Y, Elston TC, Dohlman HG, Control of MAPK specificity by feedback phosphorylation of shared adaptor protein Ste50. J. Biol. Chem. 283, 33798–802 (2008). [PubMed: 18854322]
26. Clement ST, Dixit G, Dohlman HG, Regulation of yeast G protein signaling by the kinases that activate the AMPK homolog Snf1. Sci. Signal. 6, ra78 (2013).
27. Isom D, Sridharan V, Baker R, Clement S, Smalley D, Dohlman H, Protons as second messenger regulators of G protein signaling. Mol. Cell. 51, 531–538 (2013). [PubMed: 23954348]
28. Miesenböck G, De Angelis DA, Rothman JE, Visualizing secretion and synaptic transmission with pH-sensitive green fluorescent proteins. Nature. 394, 192–195 (1998). [PubMed: 9671304]
29. Brett CL, Tukaye DN, Mukherjee S, Rao R, The yeast endosomal Na+K+/H+ exchanger Nhx1 regulates cellular pH to control vesicle trafficking. Mol. Biol. Cell. 16, 1396–405 (2005). [PubMed: 15635088]
30. Claret S, Gatti X, Doignon F, Thoraval D, Crouzet M, The Rgd1p Rho GTPase-Activating Protein and the Mid2p Cell Wall Sensor Are Required at Low pH for Protein Kinase C Pathway Activation and Cell Survival in Saccharomyces cerevisiae. Eukaryot. Cell. 4, 1375–1386 (2005). [PubMed: 16087742]
31. van Drogen F, Mishra R, Rudolf F, Walczak MJ, Lee SS, Reiter W, Hegemann B, Pelet S, Dohnal I, Binolfi A, Yudina Z, Selenko P, Wider G, Ammerer G, Peter M, Mechanical stress impairs pheromone signaling via Pkc1-mediated regulation of the MAPK scaffold Ste5. J. Cell Biol. 218, 3117–3133 (2019). [PubMed: 31315942]
32. Kreegipuu A, Blom N, Brunak S, Järv J, Statistical analysis of protein kinase specificity determinants. FEBS Lett. 430, 45–50 (1998). [PubMed: 9678592]
33. Taverna SD, Ilin S, Rogers RS, Tanny JC, Lavender H, Li H, Baker L, Boyle J, Blair LP, Chait BTT, Patel DJ, Aitchison JD, Tackett AJ, Allis CD, Yng1 PHD Finger Binding to H3 Trimethylated at K4 Promotes NuA3 HAT Activity at K14 of H3 and Transcription at a Subset of Targeted ORFs. Mol. Cell. 24, 785–796 (2006). [PubMed: 17157260]
34. Maltby VE, Martin BJE, Brind'Amour J, Chruscicki AT, McBurney KL, Schulze JM, Johnson IJ, Hills M, Hentrich T, Kobor MS, Lorincz MC, Howe LJ, Histone H3K4 demethylation is negatively regulated by histone H3 acetylation in Saccharomyces cerevisiae. Proc. Natl. Acad. Sci. 109, 18505–18510 (2012). [PubMed: 23091032]

35. Sakaguchi K, Herrera JE, Saito S, Miki T, Bustin M, Vassilev A, Anderson CW, Appella E, DNA damage activates p53 through a phosphorylation-acetylation cascade. Genes Dev. 12, 2831–41 (1998). [PubMed: 9744860]
36. Hicke L, Zanolari B, Riezman H, Cytoplasmic tail phosphorylation of the alpha-factor receptor is required for its ubiquitination and internalization. J. Cell Biol. 141, 349–58 (1998). [PubMed: 9548714]
37. Darling AL, Uversky VN, Intrinsic disorder and posttranslational modifications: The darker side of the biological dark matter. Front. Genet. 9, 1–18 (2018). [PubMed: 29387083]
38. Pejaver V, Hsu WL, Xin F, Dunker AK, Uversky VN, Radivojac P, The structural and functional signatures of proteins that undergo multiple events of post-translational modification. Protein Sci. 23, 1077–1093 (2014). [PubMed: 24888500]
39. Bah A, Vernon RM, Siddiqui Z, Krzeminski M, Muhandiram R, Zhao C, Sonenberg N, Kay LE, Forman-Kay JD, Folding of an intrinsically disordered protein by phosphorylation as a regulatory switch. Nature. 519, 106–9 (2015). [PubMed: 25533957]
40. Bhattacharyya RP, Reményi A, Good MC, Bashor CJ, Falick AM, a Lim W, The Ste5 scaffold allosterically modulates signaling output of the yeast mating pathway. Science. 311, 822–6 (2006). [PubMed: 16424299]
41. Hao N, Nayak S, Behar M, Shanks RH, Nagiec MJ, Errede B, Hasty J, Elston TC, Dohlman HG, Regulation of cell signaling dynamics by the protein kinase-scaffold Ste5. Mol. Cell. 30, 649–56 (2008). [PubMed: 18538663]
42. Brewster JL, de Valoir T, Dwyer ND, Winter E, Gustin MC, An osmosensing signal transduction pathway in yeast. Science. 259, 1760–3 (1993). [PubMed: 7681220]
43. Mok J, Kim PM, Lam HYK, Piccirillo S, Zhou X, Jeschke GR, Sheridan DL, Parker SA, Desai V, Jwa M, Cameroni E, Niu H, Good M, Remenyi A, Ma J-LN, Sheu Y-J, Sassi HE, Sopko R, Chan CSM, De Virgilio C, Hollingsworth NM, Lim WA, Stern DF, Stillman B, Andrews BJ, Gerstein MB, Snyder M, Turk BE, Deciphering protein kinase specificity through large-scale analysis of yeast phosphorylation site motifs. Sci. Signal. 3, ra12 (2010).
44. Hong SP, Leiper FC, Woods A, Carling D, Carlson M, Activation of yeast Snf1 and mammalian AMP-activated protein kinase by upstream kinases. Proc. Natl. Acad. Sci. U. S. A. 100, 8839–8843 (2003). [PubMed: 12847291]
45. Stack JH, Herman PK, Schu PV, Emr SD, A membrane-associated complex containing the Vps15 protein kinase and the Vps34 PI 3-kinase is essential for protein sorting to the yeast lysosome-like vacuole. EMBO J. 12, 2195–2204 (1993). [PubMed: 8387919]
46. Stack JH, DeWald DB, Takegawa K, Emr SD, Vesicle-mediated protein transport: Regulatory interactions between the Vps15 protein kinase and the Vps34 PtdIns 3-kinase essential for protein sorting to the vacuole in yeast. J. Cell Biol. 129, 321–334 (1995). [PubMed: 7721937]
47. Tanigawa M, Maeda T, An In Vitro TORC1 Kinase Assay That Recapitulates the Gtr-Independent Glutamine-Responsive TORC1 Activation Mechanism on Yeast Vacuoles. Mol. Cell. Biol. 37, 1–16 (2017).
48. Kihara A, Noda T, Ishihara N, Ohsumi Y, Two distinct Vps34 phosphatidylinositol 3-kinase complexes function in autophagy and carboxypeptidase y sorting in Saccharomyces cerevisiae. J. Cell Biol. 153, 519–530 (2001).
49. Sambade M, Alba M, Smardon AM, West RW, Kane PM, A genomic screen for yeast vacuolar membrane ATPase mutants. Genetics. 170, 1539–51 (2005). [PubMed: 15937126]
50. Slessareva JE, Routt SM, Temple B, Bankaitis VA, Dohlman HG, Activation of the phosphatidylinositol 3-kinase Vps34 by a G protein alpha subunit at the endosome. Cell. 126, 191–203 (2006). [PubMed: 16839886]
51. Isom DG, Dohlman HG, Buried ionizable networks are an ancient hallmark of G protein-coupled receptor activation. Proc. Natl. Acad. Sci. 112, 5702–5707 (2015). [PubMed: 25902551]
52. Isom DG, Page SC, Collins LB, Kapolka NJ, Taghon GJ, Dohlman HG, Coordinated regulation of intracellular pH by two glucose-sensing pathways in yeast. J. Biol. Chem. 293, 2318–2329 (2018). [PubMed: 29284676]
53. Smrcka AV, G protein beta gamma subunits: Central mediators of G protein-coupled receptor signaling. Cell. Mol. Life Sci. 65, 2191–2214 (2008). [PubMed: 18488142]

54. English N, Torres M, SAPH-ire TFx: A Machine Learning Recommendation Method and Webtool for the Prediction of Functional Post-Translational Modifications. bioRxiv (2019), doi:10.1101/731026.
55. Storici F, a Resnick M, The delitto perfetto approach to in vivo site-directed mutagenesis and chromosome rearrangements with synthetic oligonucleotides in yeast. Methods Enzymol. 409, 329–45 (2006). [PubMed: 16793410]
56. Levin DE, Bartlett-Heubusch E, Mutants in the Scerevisiae PKC1 gene display a cell cycle-specific osmotic stability defect. J. Cell Biol. 116, 1221–1229 (1992). [PubMed: 1740473]
57. Inagaki M, Schmelzle T, Yamaguchi K, Irie K, Hall MN, Matsumoto K, PDK1 homologs activate the Pkc1-mitogen-activated protein kinase pathway in yeast. Mol. Cell. Biol. 19, 8344–52 (1999). [PubMed: 10567559]
58. Robinson LC, Menold MM, Garrett S, Culbertson MR, Casein kinase I-like protein kinases encoded by YCK1 and YCK2 are required for yeast morphogenesis. Mol. Cell. Biol. 13, 2870–2881 (1993). [PubMed: 8474447]
59. Li MZ, Elledge SJ, Harnessing homologous recombination in vitro to generate recombinant DNA via SLIC. Nat. Methods. 4, 251–6 (2007). [PubMed: 17293868]
60. Nagiec MJ, Dohlman HG, Checkpoints in a yeast differentiation pathway coordinate signaling during hyperosmotic stress. PLoS Genet. 8, e1002437 (2012). [PubMed: 22242015]
61. Lee MJ, Dohlman HG, Coactivation of G Protein Signaling by Cell-Surface Receptors and an Intracellular Exchange Factor. Curr. Biol. 18, 211–215 (2008). [PubMed: 18261907]
62. Schindelin J, Rueden CT, Hiner MC, Eliceiri KW, The ImageJ ecosystem: An open platform for biomedical image analysis. Mol. Reprod. Dev. 82, 518–529 (2015). [PubMed: 26153368]
63. Zhang Y-Q, Gamarra S, Garcia-Effron G, Park S, Perlin DS, Rao R, Requirement for ergosterol in V-ATPase function underlies antifungal activity of azole drugs. PLoS Pathog. 6, e1000939 (2010). [PubMed: 20532216]
64. Phillips JC, Braun R, Wang W, Gumbart J, Tajkhorshid E, Villa E, Chipot C, Skeel RD, Kalé L, Schulten K, Scalable molecular dynamics with NAMD. J. Comput. Chem. 26, 1781–1802 (2005). [PubMed: 16222654]
65. Case DA, Betz RM, Cerutti DS, C. I. T.E., Darden TA, Duke RE, Giese TJ, Gohlke H, Goetz AW, Homeyer N, Izadi S, Janowski P, Kaus J, Kovalenko A, Lee TS, LeGrand S, Li P, Lin C, Luchko T, Luo R, Madej B, Mermelstein D, Merz KM, Monard G, Nguyen H, Nguyen HT, Omelyan I, Onufriev A, Roe DR, Roitberg A, Sagui C, Simmerling CL, Botello-Smith WM, Swails J, Walker RC, Wang J, Wolf RM, Wu X, Xiao L, Kollman PA, Amber 2016. Univ. California, San Fr. (2016).
66. Piana S, Lindorff-Larsen K, Shaw DE, How Robust Are Protein Folding Simulations with Respect to Force Field Parameterization?Biophys. J. 100, L47–L49 (2011). [PubMed: 21539772]
67. Best RB, Zhu X, Shim J, Lopes PEM, Mittal J, Feig M, MacKerell AD, Optimization of the Additive CHARMM All-Atom Protein Force Field Targeting Improved Sampling of the Backbone ϕ, ψ and Side-Chain χ 1 and χ 2 Dihedral Angles. J. Chem. Theory Comput. 8, 3257–3273 (2012). [PubMed: 23341755]
68. Jorgensen WL, Chandrasekhar J, Madura JD, Impey RW, Klein ML, Comparison of simple potential functions for simulating liquid water. J. Chem. Phys. 79, 926–935 (1983).
69. Humphrey W, Dalke A, Schulten K, VMD: Visual molecular dynamics. J. Mol. Graph. 14, 33–38 (1996). [PubMed: 8744570]
70. Feller SE, Zhang Y, Pastor RW, Brooks BR, Constant pressure molecular dynamics simulation: The Langevin piston method. J. Chem. Phys. 103, 4613–4621 (1995).
71. Hopkins CW, Le Grand S, Walker RC, Roitberg AE, Long-Time-Step Molecular Dynamics through Hydrogen Mass Repartitioning. J. Chem. Theory Comput. 11, 1864–1874 (2015). [PubMed: 26574392]
72. Balusek C, Hwang H, Lau CH, Lundquist K, Hazel A, Pavlova A, Lynch DL, Reggio PH, Wang Y, Gumbart JC, Accelerating Membrane Simulations with Hydrogen Mass Repartitioning. J. Chem. Theory Comput. 15, 4673–4686 (2019). [PubMed: 31265271]
73. Darden T, York D, Pedersen L, Particle mesh Ewald: An N ·log(N) method for Ewald sums in large systems. J. Chem. Phys. 98, 10089–10092 (1993).

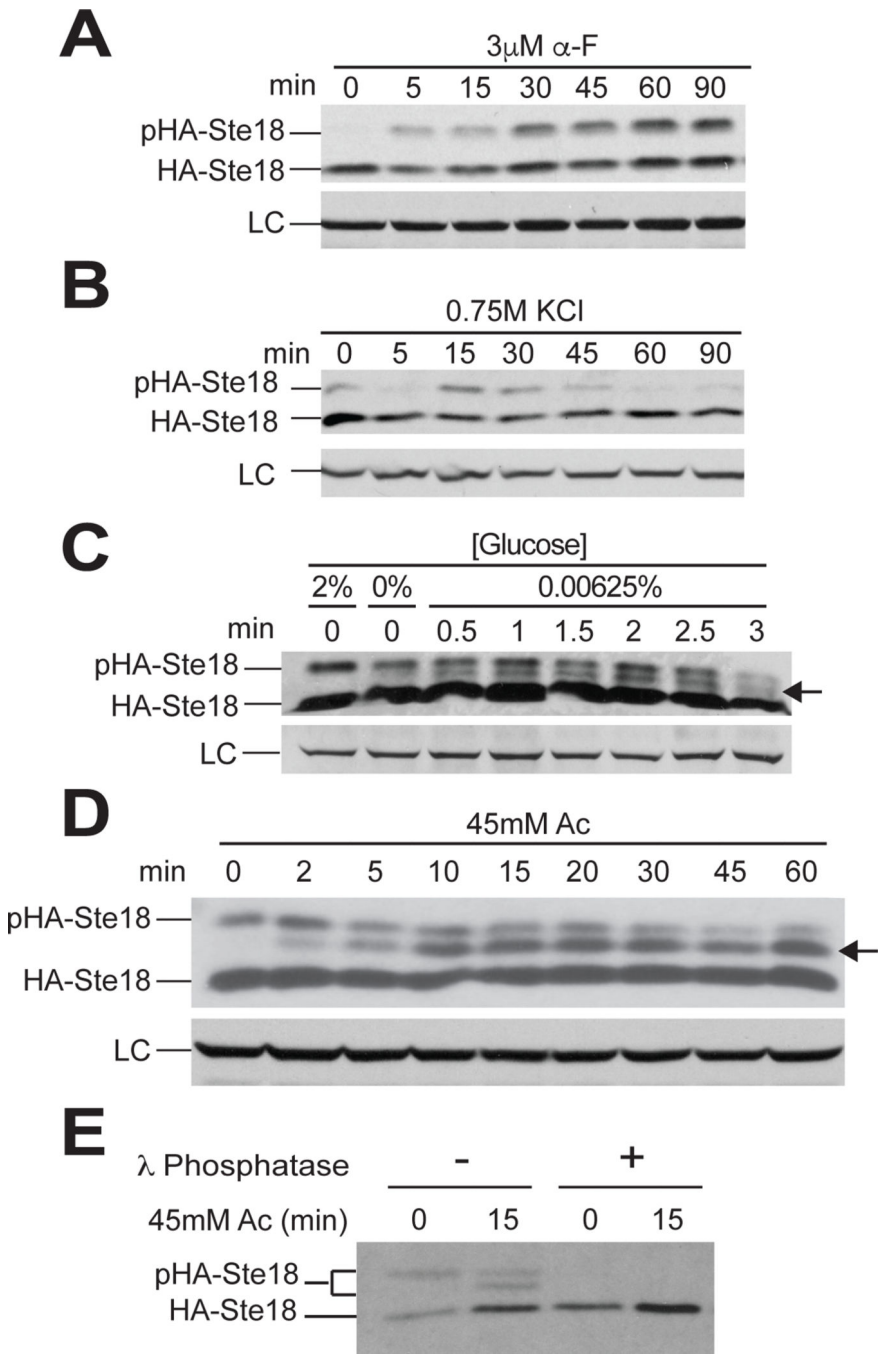

Fig. 1. Ste18 is phosphorylated in response to cell stress.

(**A** to **D**) The phosphorylation-dependent electrophoretic mobility of HA-Ste18 was monitored by Western blotting with an anti-HA antibody. Cells were analyzed after exposure to 3 μM α-factor mating pheromone (α-F) for the indicated times (A), 0.75 M potassium chloride for the indicated times (B), 0, 0.00625 (low), or 2% (standard) glucose (C), or 45 mM acetic acid (Ac) for the indicated times (D). (**E**) Protein extracts of cells exposed to acid stress (45 mM acetic acid for 15 min) were treated with or without alkaline phosphatase to establish the dependence of each mobility-shifted band on phosphorylation.

LC, loading control (yeast G6PDH); pHA-Ste18, phosphorylated HA-Ste18. Western blots are representative of three experiments, except for (E), which is from a single experiment. Arrows to the right of the blots indicate a middle band found between the bottom and top bands observed under conditions of glucose or acetic acid stress.

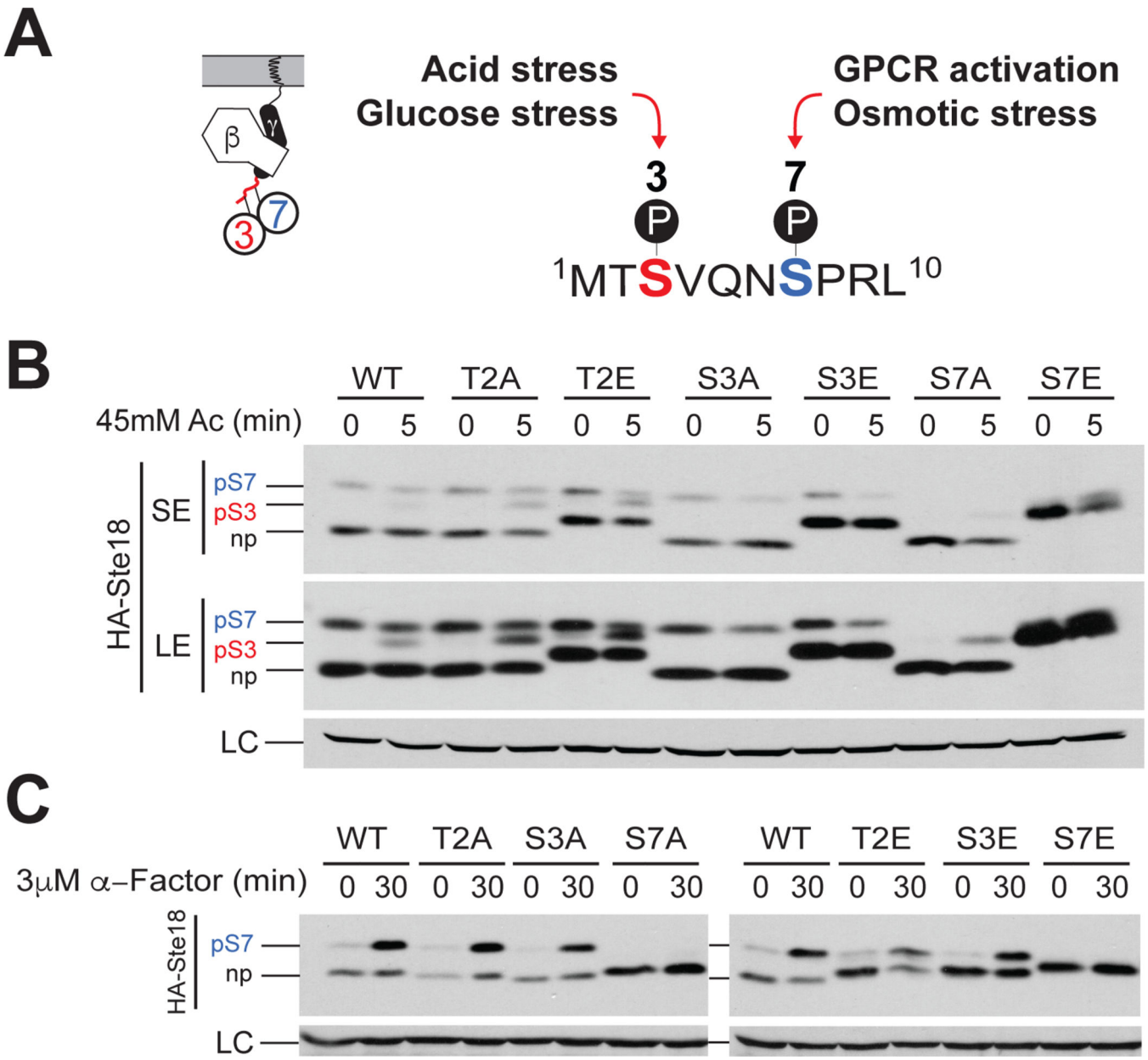

Fig. 2. pH- and pheromone-dependent phosphorylations occur at distinct phosphorylation sites in Ste18^{Nt}.

(**A**) Schematic summary of site-specific phosphorylation events and their corresponding stimuli across the intrinsically disordered N-terminal tail of Ste18. (**B** and **C**) Cells harboring WT Ste18 or the indicated single-phosphosite mutations in Ste18 were left untreated (0) or were treated with 45 mM acetic acid (Ac) for 5 min (B) or with 3 μM pheromone (α-Factor) for 30 min before being subjected to Western blotting analysis with an anti-HA antibody. As indicated, the detected bands correspond to nonphosphorylated Ste18 (np) or Ste^{Nt} phosphorylated at Ser^{7} (pS7) or Ser^{3} (pS3). Western blots are representative of two to three experiments. LC, loading control (yeast G6PDH); SE, short exposure; LE, long exposure.

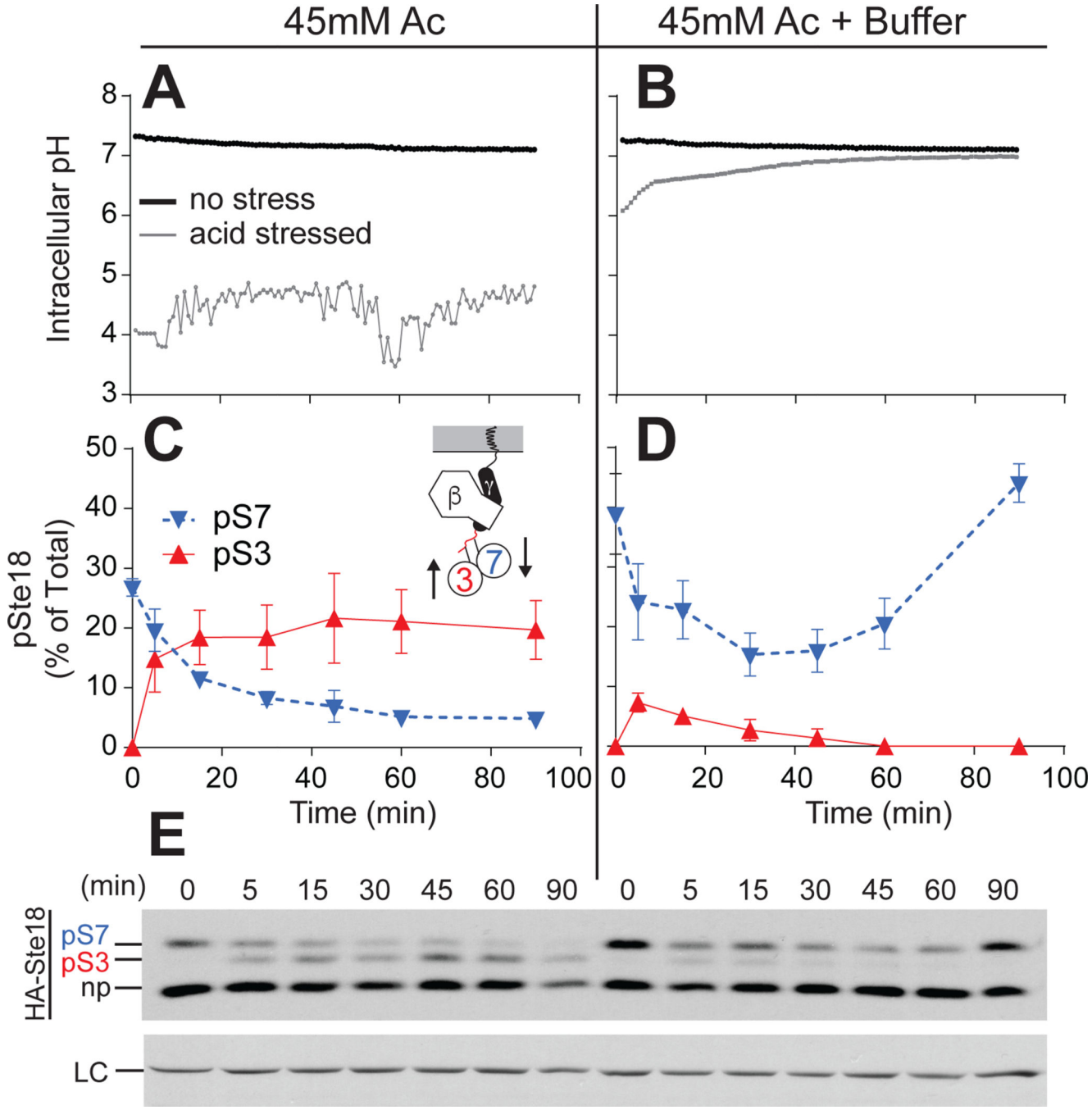

Fig. 3. Ste18^{pS3} and Ste18^{pS7} are inversely regulated in response to intracellular acidification.

(**A** to **E**) WT *BY4741* yeast cells transformed with a pH-sensitive pHluorin probe were left untreated or were incubated for the indicated times with 45 mM acetic acid (Ac) in the absence or presence of buffer. (A and B) Intracellular pH was monitored over time. The relative abundances of Ste18 phosphorylated at S7 (pS7) and S3 (pS3) under the indicated conditions were determined by quantitative analysis of Western blotting data (C and D). (E) Representative Western blotting analysis of Ste18 phosphorylation status under

the indicated conditions. Results are means ± SD (n = 4 experiments). LC, loading control (yeast G6PDH).

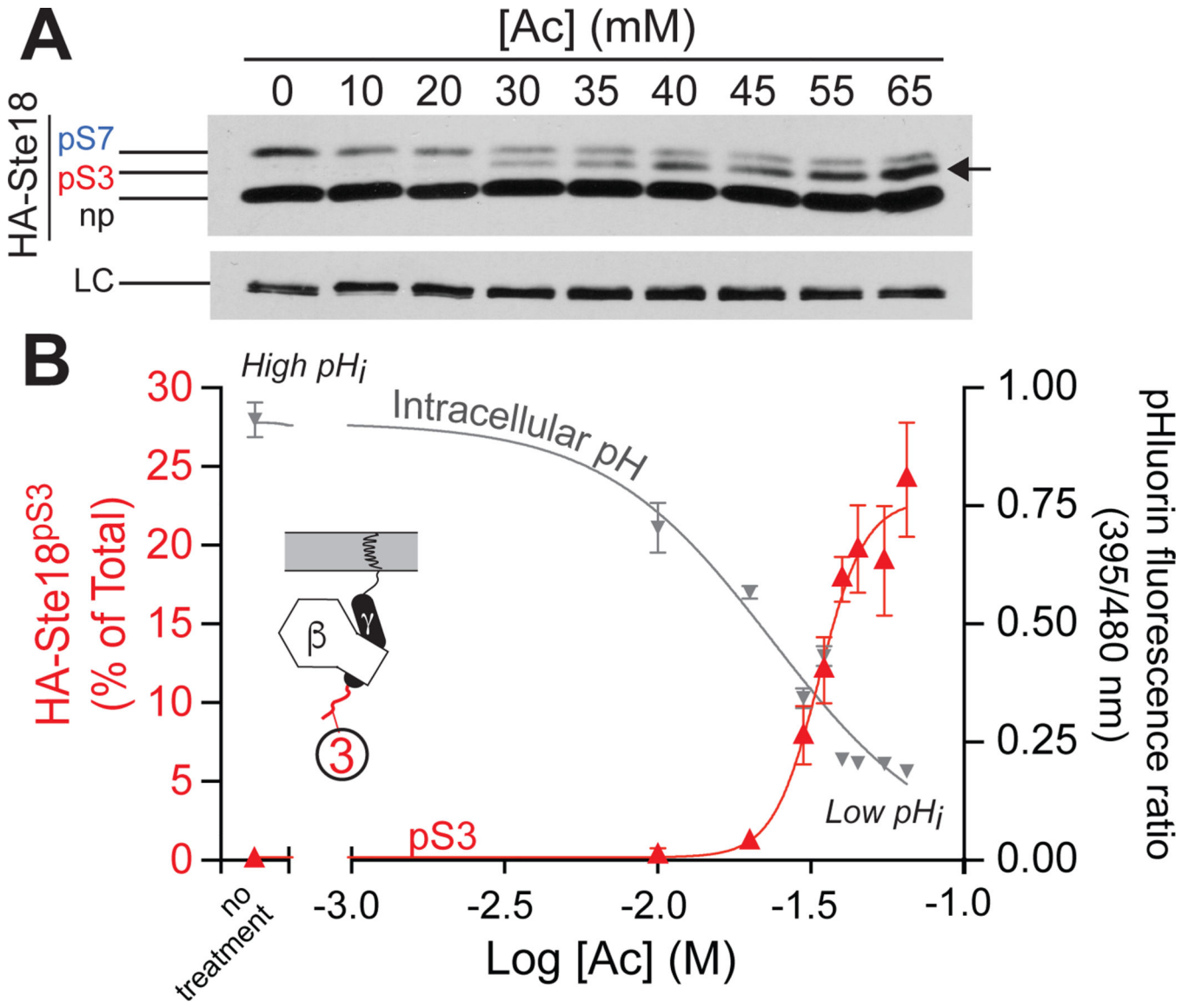

Fig. 4. Ste18^{pS3} is a pH indicator.

(**A**) Representative Western blot showing Ste18^{Nt} phosphorylation after a 15-min exposure to the indicated concentrations of acetic acid (Ac) in the absence of buffer. pS7, Ste18 phosphorylation at Ser^{7}; pS3, Ste18 phosphorylation at Ser^{3}; np, nonphosphorylated Ste18. LC, loading control (yeast G6PDH). (**B**) Analysis of the relative abundance of Ste18^{pS3} (red trace) and the ratio of fluorescence intensities emitted upon excitation of pHluorin at 395 and 480 nm as a function of acetic acid concentration (gray). Cells were collected 15 min after acetic acid treatment to trap the maximal phosphorylation state of Ste18. Results are means ± SEM (n = 4 experiments).

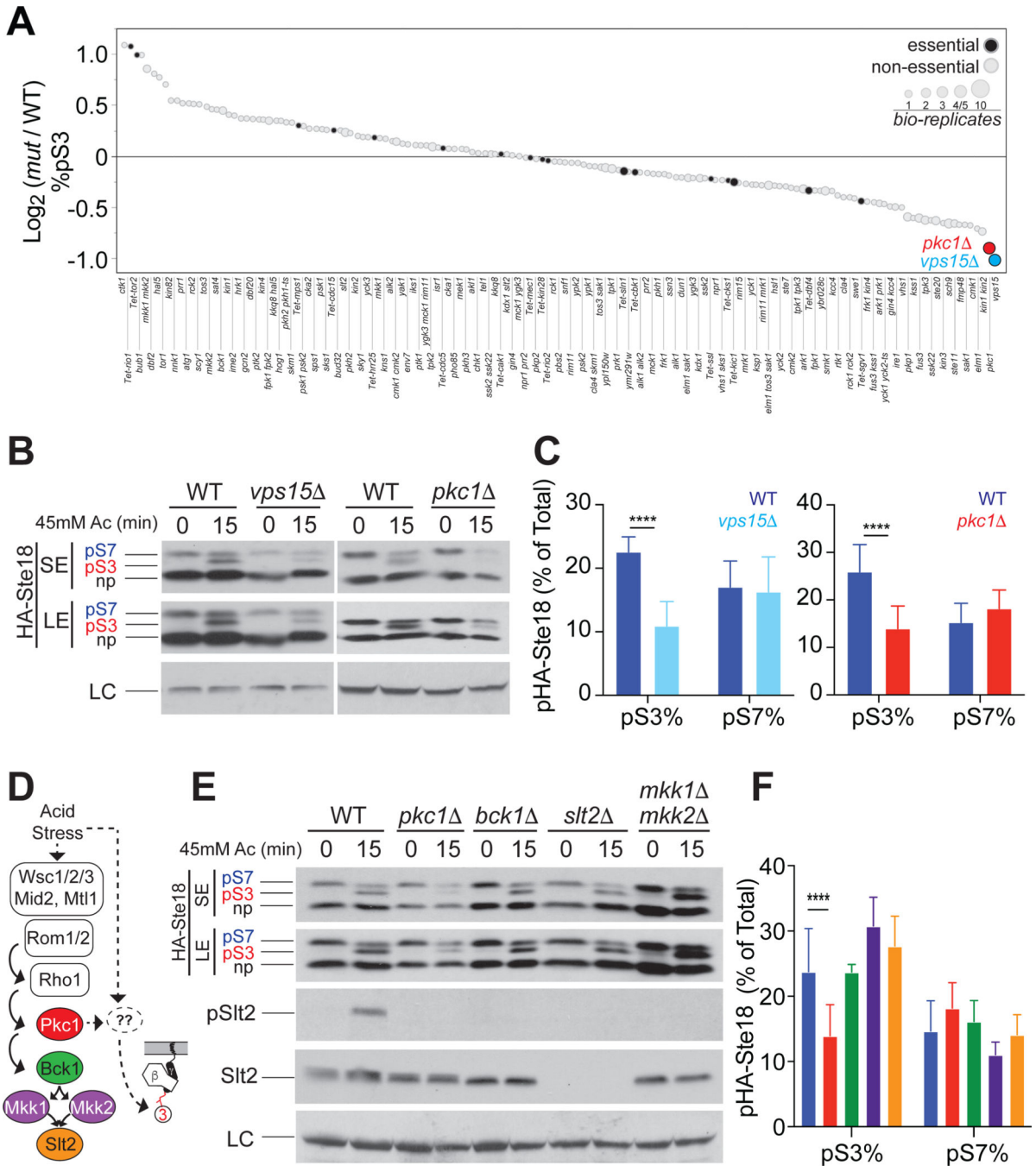

Fig. 5. Vps15 and Pkc1, but not the CWI pathway, are necessary for maximal phosphorylation of Ste18^{S3} in response to acid stress.

(**A** to **C**) WT or the indicated mutant yeast strains transformed with *pRS31x-HA-STE18* under the control of the *STE18* promoter/terminator were treated with 45 mM acetic acid without buffer for 0 or 15 minutes before being subjected to SDS-PAGE and Western blotting analysis with anti-HA antibody. (A) Plot of the relative pS3 response to acetic acid for each of 151 mutant strains. Data are plotted as Log_2 of the ratio of %pS3 in the mutant (mut) relative to the WT strain from the same experiment for single and multiple

gene deletion/mutant strains. For Tet-off strains, data are plotted as Log_2 of the ratio of the percentage of $Ste18^{pS3}$ in the mutant with doxycycline relative to mutant without doxycycline. Bio-replicates (circle size) correspond to unique single colonies tested. (B) Representative Western blots for *vps15Δ* and *pkc1Δ* cells relative to WT cells in response to exposure to 45 mM acetic acid for the indicated times. (C) Quantification of the relative percentages of $Ste18^{pS3}$ and $Ste18^{pS7}$ measured across 10 biological replicate experiments as shown in (B). (**D**) Schematic diagram of the CWI pathway. (**E**) Representative Western blotting analysis of HA-Ste18 in WT or the indicated CWI pathway kinase gene deletion strains after treatment for the indicated times with 45 mM acetic acid without buffer. (**F**) Quantification of the relative percentages of $Ste18^{pS3}$ and $Ste18^{pS7}$ from the experiments represented in (E). pSlt2, phosphorylated Slt2. LC, loading control (yeast G6PDH). For all quantitative analyses, data are means ± SD from four to 10 biological and analytical replicates. Statistical significance was determined relative to the WT strain by two-way ANOVA with Sidak's test for post-hoc multiple-comparisons analysis using nonsaturated exposures. **** $P < 0.0001$. SE, short exposure; LE, long exposure.

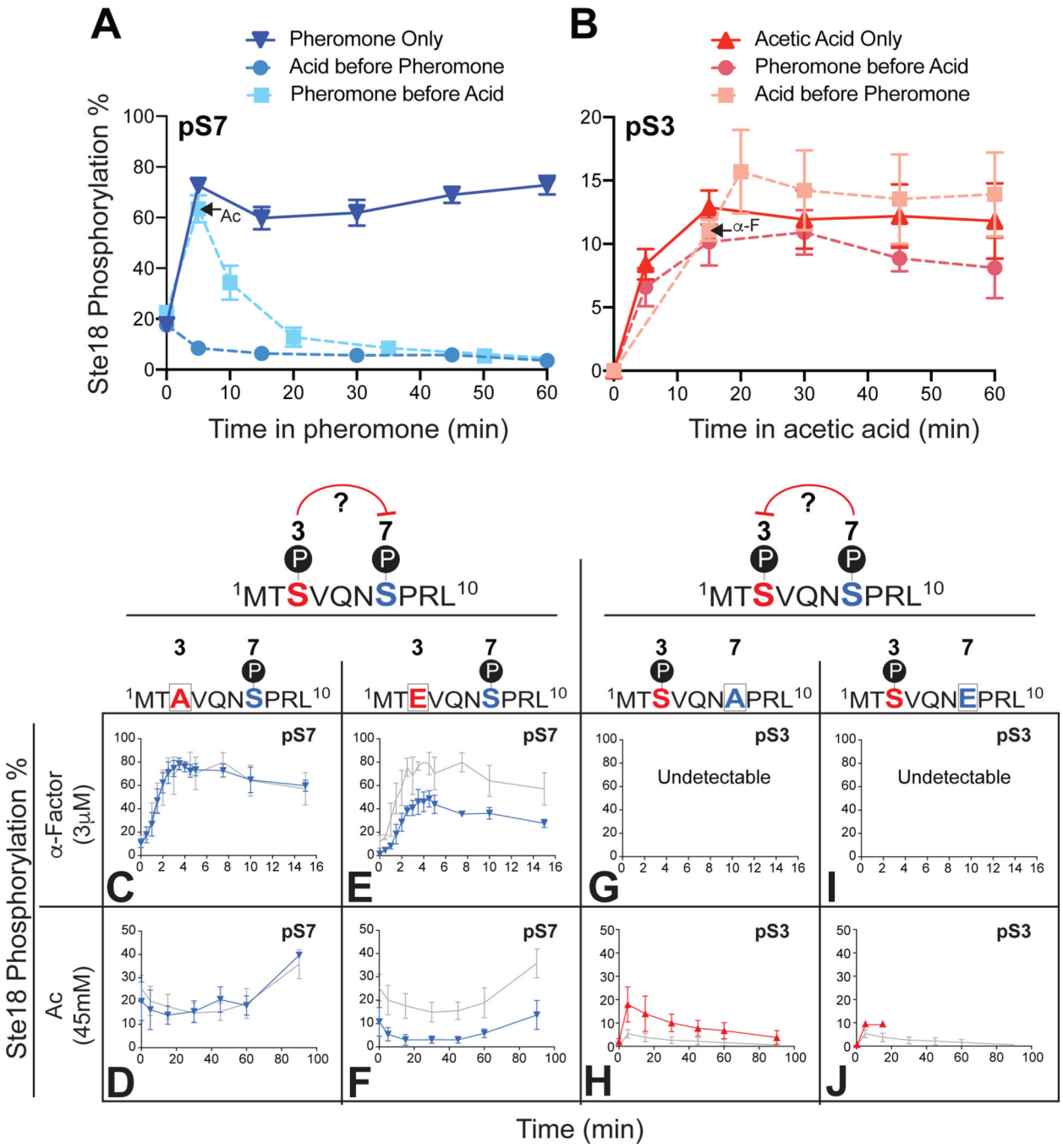

Fig. 6. Costimulation and site-specific substitutions reveal interactions between Ste18^{pS3} and Ste18^{pS7}.

(**A**) Analysis of the change in Ste18^{pS7} abundance in response to pheromone, pheromone after a 15-min pretreatment with 45 mM acetic acid, or pheromone before post-treatment with 45 mM acetic acid. The black arrow indicates the time of acetic acid post-treatment. (**B**) Analysis of the change in Ste18^{pS3} abundance in response to 45 mM acetic acid, acetic acid after a 5-min pretreatment with 3 μM α-factor (α-F), or acetic acid before post-treatment with 3 μM α-F. The black arrow indicates the time of α-F post-treatment. For

(A) and (B), cultures were unbuffered for all experiments. (**C** to **J**) The relative abundances of Ste18^{pS3} and Ste18^{pS7} were measured by quantitative Western blotting analysis of yeast cells endogenously expressing WT Ste18 or the indicated Ste18 phosphosite mutants and then exposed to 3 μM pheromone or 45 mM acetic acid in buffered medium for 15 or 90 min, respectively. (C to F) Quantification of Ste18^{pS7} abundance with respect to S3A and S3E under the indicated conditions (blue). (G to J) Quantification of Ste18^{pS3} abundance with respect to S7A and S7E under the indicated conditions (red). WT responses (means ± SD) across all experiments for each respective phosphosite in Ste18 wherein S3 and S7 were undisrupted are shown with gray lines (n = 6 experiments). Mutant results are means ± SD (n = 4 to 6 experiments) for all but (J, pS3) (n = 1). For (E) and (F), all but one time point pair (WT vs. mutant) beyond t = 5 min were determined to be significantly different ($P < 0.05$). For (H), significant differences ($P < 0.05$) were only found for 5, 15, and 30 min. Statistical significance was determined by two-way ANOVA with a Bonferroni post-hoc test for multiple comparisons. See figs. S3 and S4 for representative Western blot images.

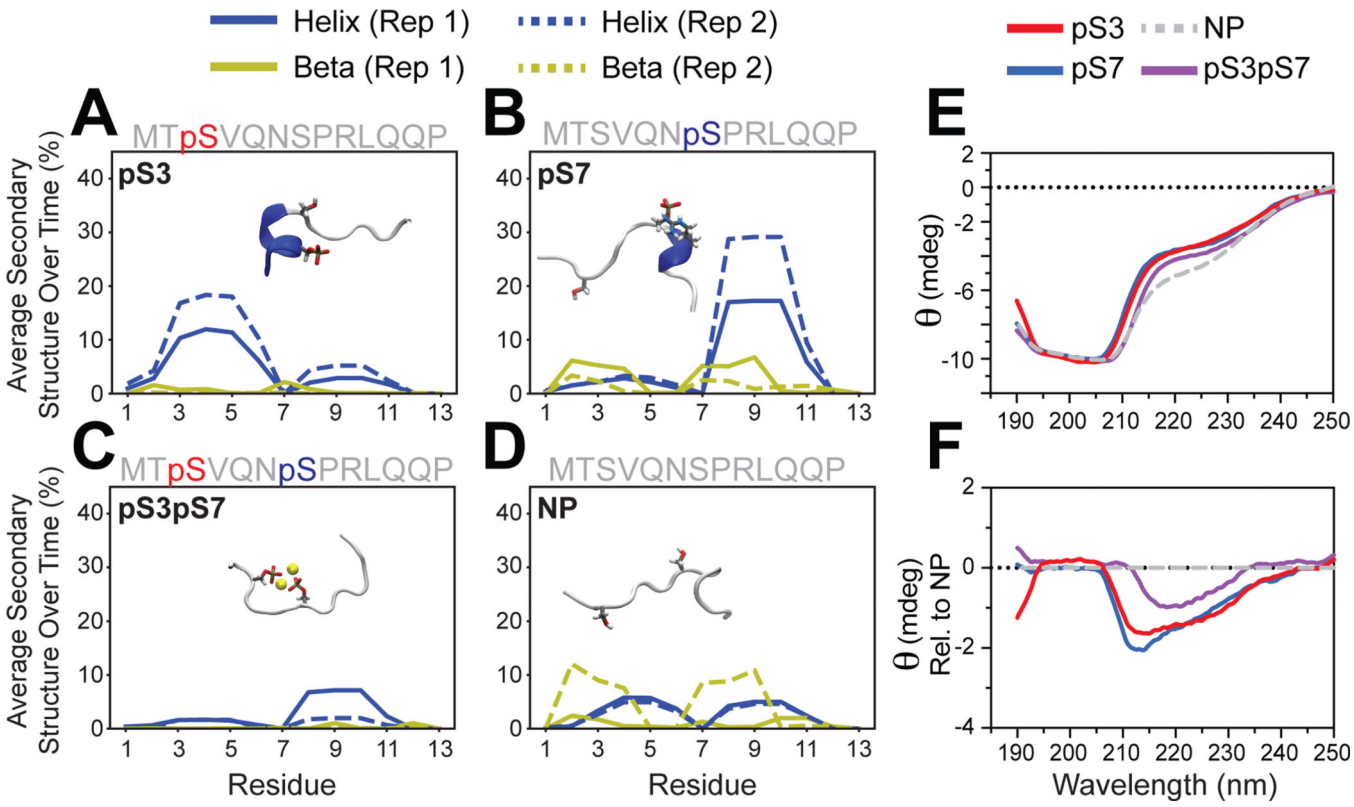

Fig. 7. Phosphorylation promotes changes in the Ste18^{Nt} IDR structure.

(**A** to **D**) Two independent MD simulations for synthetic pS3, pS7, pS3pS7, and nonphosphorylated (NP) peptides. Plots show the average secondary structure percentage (alpha helix or beta hairpin) relative to the amino acid position in each peptide (see fig. S7 for independent time traces). Insets show representative structures of the respective Ste18^{Nt} peptides. (**E**) CD spectrum of synthetic nonphosphorylated (NP) and phosphorylated Ste18^{Nt} peptides. Peptides were N-terminally acetylated and C-terminally amidated to prevent N- and C-terminal charge interactions that would not be possible within the N-terminus of the protein. (**F**) Difference CD spectra from (E) showing deviations between each phosphopeptide relative to the nonphosphorylated form.

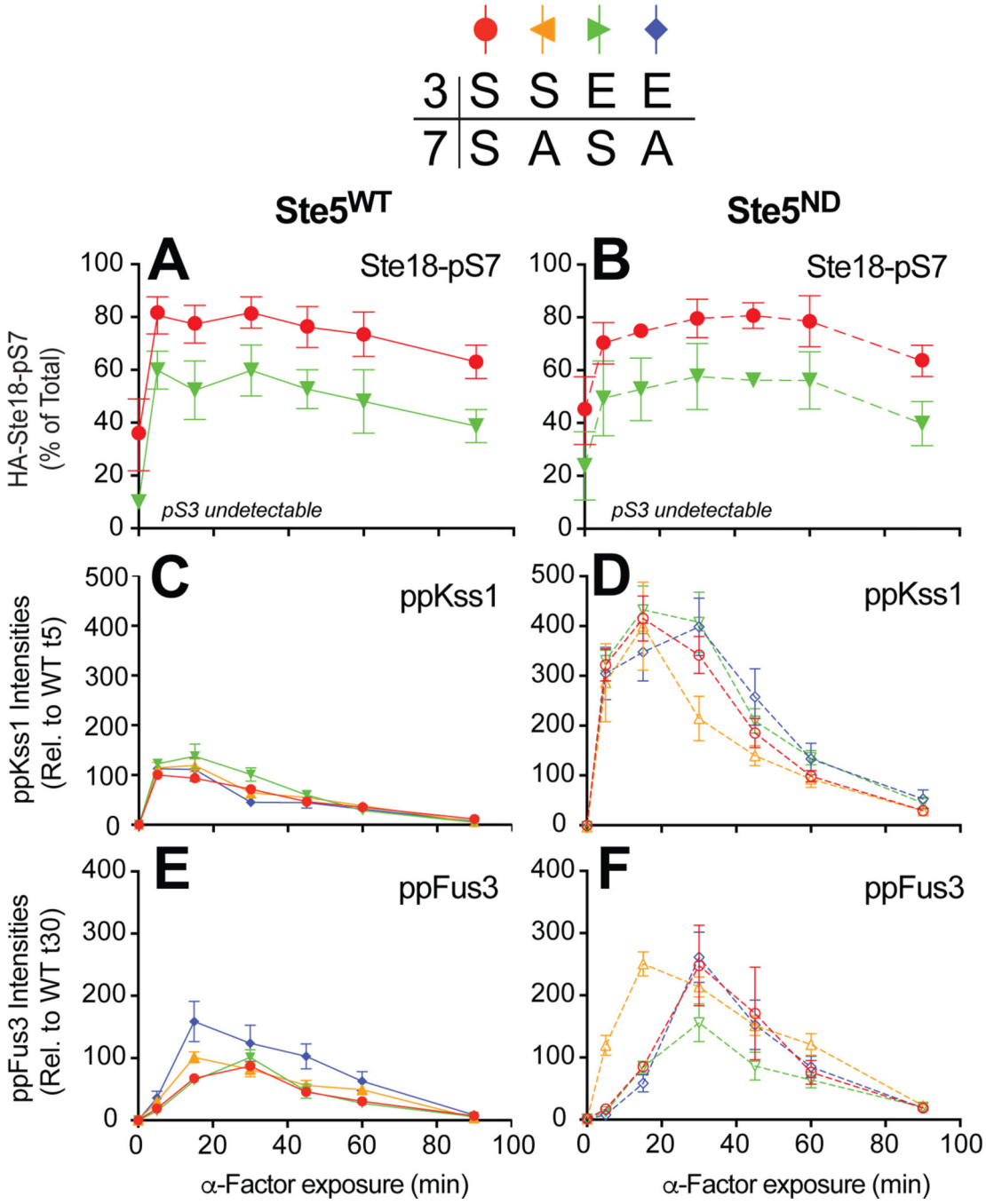

Fig. 8. Combinatorial phosphorylation on Ste18^{pS3} and Ste18^{pS7} controls the activation rate and amplitude of the MAPK Fus3.

(**A** to **F**) Fus3 activation is a hypersensitive diagnostic for the effects of Ste18^{Nt} phosphorylation when combined with Ste5 mutants lacking a functional Fus3-binding domain (Ste5ND) (18), and was used to evaluate combinatorial phosphorylation states. Yeast strains endogenously expressing Ste5^{WT} or Ste5ND and one of four Ste18 phosphosite isoforms (S3/S7, S3/A7, E3/S7, E3/A7) were exposed to pheromone for 90 min with sampling for Western blotting analysis of HA-Ste18, activated Kss1 (ppKss1), and activated

Fus3 (ppFus3), as indicated. (A and B) Relative abundance of $Ste18^{pS7}$ in $Ste5^{WT}$ (A) and $Ste5^{ND}$ (B) cells. (C and D) Time-resolved activation of Kss1 in $Ste5^{WT}$ (C) and $Ste5^{ND}$ (D) cells. (E and F) Time-resolved activation of Fus3 in $Ste5^{WT}$ (E) and $Ste5^{ND}$ (F) cells. Results are means ± SEM (n = 8 experiments). See fig. S8 for representative Western blot images.